Journal of Advanced Research in Fluid Mechanics and Thermal Sciences

Journal homepage:
https://semarakilmu.com.my/journals/index.php/fluid_mechanics_thermal_sciences/index
ISSN: 2289-7879

The Consequences of Thermal Radiation and Chemical Reactions on Magneto-hydrodynamics in Two Dimensions over a Stretching Sheet with Jeffrey Fluid

Vijay K. Patel[1,*], Jigisha U. Pandya[2]

[1] Department of Mathematics, LDRP Institute of Technology and Research, Kadi Sarva Vishwavidyalaya, Gandhinagar, 382015, Gujarat, India
[2] Department of Mathematics, Sarvajanik College of Engineering and Technology, Gujarat Technological University, Surat, 395001, Gujarat, India

ARTICLE INFO

Article history:
Received 13 January 2022
Received in revised form 5 April 2022
Accepted 10 April 2022
Available online 13 May 2022

Keywords:
Fluid dynamics; heat transfer; numerical simulation; Homotopy Analysis Method; magneto-hydrodynamics; stretching sheet; Jeffrey fluid; chemical reactors thermal radiation

ABSTRACT

The Homotopy Analysis Method is employed in this research study to analyse the two-dimensional electrical conduction of a magnetohydrodynamic (MHD) Jeffrey fluid flow over a stretched sheet under various conditions. The governing partial differential equation is transformed into terms of nonlinear coupled ordinary differential equations via a similarity transformation. A system of ordinary differential equations is solved and the effect of various numerical values on velocity, concentration, and temperature is investigated and shown in tables and graphs. It is observed that the Deborah number (β) and the ratio of relaxation and retardation times parameter (λ_2) have diametrically opposed impacts on the skin friction coefficient. Consequently, the effects of Pr and β on the Nusselt number profiles are comparable. Therefore, the current findings correlate with those obtained for a viscous fluid. Calculations for the Homotopy Analysis Method were performed on the PARAM Shavak high-performance computing (HPC) computer using the BVPh2.0 Mathematica tool.

1. Introduction

Recently, owing to its numerous uses in manufacturing and industry, the study of boundary layer flow over a stretched sheet has captured the attention of magneto-hydrodynamics experts. This assortment of different manufacturing processes includes a process for drawing copper wire, an infinitely long metal plate in a cooling bath, the polymer extrusion process, and plastic film stretch production. The surface condition or roughness is essential to determine the heat transfer rate when the cooling of hot metals can control the mechanical and physical properties of the final product. The introduction of the concept of continuous solid surface boundary layer flow was given by Sakiadis [1]. Crane [2] supplied the standard solution of a sheet that moves with a linear change in velocity and distance from a fixed point in a viscous fluid's boundary layer flow. Merkin *et al.,* [3] investigated the boundary layer flow issue in unsteady magneto-hydrodynamics (MHD). When Sheikholeslami *et*

* *Corresponding author.*
E-mail address: vijay.research351@gmail.com

https://doi.org/10.37934/arfmts.95.1.121144

al., [4] performed their study, they utilized the Homotopy Analysis Method to estimate heat transfer flow and magneto-hydrodynamics inside a rotating system. Ashorynejad *et al.,* [5] examined the effect of magnetic fields on nano-fluid heat transfer and flowed inside a stretched cylinder. Cortell [6] examined the effects of heat radiation on flow as affected by a non-linearly stretched sheet. Akbar *et al.,* [7] investigated a theoretically computed stagnant point flow effect in the presence of a shrinking plate for the Prandtl flow model with a magnetic field. Nourazar *et al.,* [8] investigated the flow of nano-fluid in the permeable cylinder employed in MHD. Nagendramma *et al.,* [9] discovered the doubly stratified magneto-hydrodynamics incompressible tangent hyperbolic nano-fluid caused by a stretched cylinder. Khan *et al.,* [10] explored Maxwell fluid upper convected flow over a stretched linear sheet as viscosity, temperature, solar radiation, and viscous despair. Waqas *et al.,* [11] investigated Jeffrey nano-material mixed convection flow, heat generation, and thermal radiation to simulate energy expression. Dawar *et al.,* [12] used homotopy analysis to study how Lorentz forces affect the flow of Jeffrey nano-fluids over a flat surface.

The non-Newtonian fluid analysis is significant because of several applications in engineering and industrial because of the flexibility of fluid properties in nature [13–23]. There are many applications, such as crystal growing, drilling mud, cosmetic products, electronics chips, food processing, and dilute polymer solutions. The non-Newtonian fluids have different rheological properties. There is no single connection between strain rate and stress that can be used to assess non-Newtonian fluids. The Jeffrey model is a simple non-Newtonian viscoelastic fluid model that is very simple to control for rheological effects. The magnetohydrodynamics nonlinear heat transfer and fluid flow over stretching sheet explored by Cortell, [24]. Bhatti *et al.,* [25] studied heat transmission by analysing solid particle motion in a dusty Jeffery fluid with varying viscosity. Ramesh, [26] examined how joule heating and viscosity dissipation affect the Jeffrey fluid. Kahshan *et al.,* [27] studied Jeffrey fluid flow's heat and mass transfer through a porous walled channel by using perturbation methods. Khan *et al.,* [28] studied the MHD flow and heat transfer of double stratified micropolar fluid over a vertical permeable shrinking/stretching sheet with chemical reaction and heat source.

Chemical reactions have practically befitted many engineering and science disciplines for heat and mass transmission, such as evaporation of water from the skin, freezing damage to crops, chemical engineering processes, and a wet cooling tower that transmits thermal energy. Shehzad *et al.,* [29] explored the nonlinear thermal radiation nonlinear nano-fluid flow of Jeffrey in three dimensions. The effects of radiation-absorbing and chemical processes on the MHD free convection heat transfer flow of a nano-fluid confined by a semi-infinite flat plate by Venkateswarlu *et al.,* [30]. Irfan *et al.,* [31] studied the unsteady flow of Carreau due to porous shrinking or stretching sheets. In addition, they investigated the effect of the binary chemical reaction and activation energy on dual nature research. Patel *et al.,* [32] studied fluid flow behaviour in two-sided square lid driven cavity by applying finite volume method. Finally, magnetite nano-fluid Muhammad *et al.,* [33] studied MHD Carreau nano-fluid flows, including motile bacteria and under slip circumstances. Hamrelaine *et al.,* [34] explored the MHD Jeffery Hamel flow and analysed stable mixed convection in two-dimensional stagnation flows of a micropolar fluid around a vertical decreasing sheet, comparing the findings and the numerical solution. Patel *et al.,* [35] examined flow analysis of four-sided square lid driven cavity and conventional numerical solutions show that the unique solutions exist for all Reynolds numbers for both the geometries. Ismail *et al.,* [36] examined the second-grade fluid of free convection flow with mass transfer and transpiration effects. They observed the impact of the relevant parameters, including the second-grade parameter, suction/injection parameter, and modified Grashof parameter, on the velocity and concentration profiles. Roja *et al.,* [37] studied the MHD fluid flow of micropolar liquid through a porous medium with the effects of thermal radiation and thermophoresis.

Recent research [38–46] has raised significant concerns about thermal radiation, nanofluid, micro-polar fluid, viscous dissipation, chemical reaction, and other features in various flow fields. We explore the MHD Jeffrey fluid model along with other parameters in this research effort since it has been shown that it is instrumental in the sciences and engineering sectors for practical determination. It is demonstrated in several domains, such as electrochemistry, finance, electromagnetism, biochemistry, and signal processing. The electrical conducting fluid flow is a critical application of the magnetic field; the MHD effect is employed to deal with the dynamics of electrically conducted fluids. Furthermore, the MHD stream issue has played a significant role in its many applications in medical and technical disciplines. However, the attendant heat transfer problems of power-law fluids through a stretched surface in the presence of a magnetic field has received relatively less attention. The flow and heat transfer of an electrically conducting, non-Newtonian power-law Jeffery fluid across a constantly stretched sheet under the effect of a transverse magnetic field are investigated in this paper. This research paper is an attempt to provide the insight into the Homotopy Analysis Method for the MHD flow of Jeffrey fluid with chemical reaction and thermal radiation.

This study aims to simulate and investigate the effects of magnetohydrodynamics Jeffrey fluid, electrical conduction of heat source and chemical processes across a stretched continuous sheet with concentration and temperature distributions. Furthermore, essential quantities of practical significance, such as the skin friction coefficient and Nusselt number, are estimated and analysed because the skin friction coefficient is a crucial dimensionless parameter in boundary-layer flows. It specifies the fraction of the local dynamic pressure felt as shear stress on the surface. The Nusselt number is a Reynolds and Prandtl number function and an important parameter that can contribute to a better heat exchange rate. The current research examines the combined consequences of both heat and mass transport over a continuous starching sheet and thermal radiation and chemical reaction. The coupled partial differential equations governing the flow field are transformed into a nonlinear ordinary differential equations system by applying appropriate transformations. The Homotopy Analysis Method (HAM) was implemented to solve governing equations. The findings are displayed graphically and discussed accordingly.

2. Model Assumptions and Mathematical Formulation

In this two-dimensional flow of viscous conductive Jeffrey fluid on a stretch surface were considering the heat transfer, chemical reaction, and the factors of thermal radiation. A stretching sheet is considered through the x-axis with variable velocity $u = U_w\ (x)\ =\ cx$, and the $y-$ axis is perpendicular to it, as shown in Figure 1. A uniform strength magnetic field B_0 is created by the linear stretching of the sheet and the simultaneous action of two equal and opposing forces along the $x-$ axis towards the direction of flow. It's indeed stable due to the magnetic field's influence on the boundary layer fluid flow. Electrical conduction generates a negligible magnetic field.

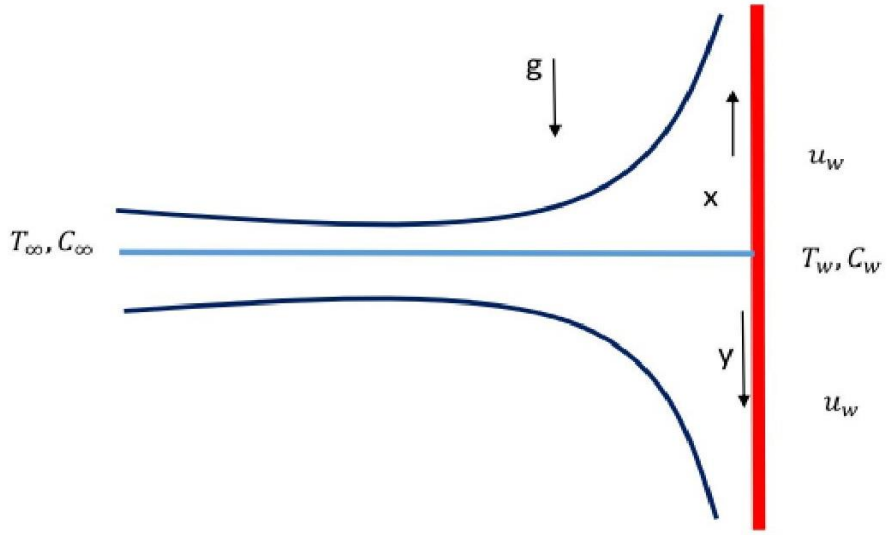

Fig. 1. The physical representation of the flow configuration and coordinate system

The Jeffrey fluid model requires an equation to be written as follows [47]

$$\tau = \mathrm{pI} + \varepsilon$$

$$\varepsilon = \frac{\mu}{(\lambda_2 + 2)}\left[R_e + \lambda_1\left(\frac{\partial R_e}{\partial t} + V \cdot \nabla\right) R_e\right]$$

where ε denotes the extra stress tensor, τ denotes the Cauchy stress tensor, μ denotes the dynamic-viscosity, λ_1 and λ_2 denote the material properties of Jeffrey fluid, R_e denotes the Rivlin‑Ericksen tensor defined by

$$R_e = (\nabla V)' + (\nabla V)$$

The following expressions are governed by the governing boundary layer equations, such as the continuity equation, momentum equation, energy with internal heat generation, thermal radiation, and concentration of species diffusion in the laminar boundary layer approximation, using the assumptions stated above as well as using standard boundary-layer approximations

$$\frac{\partial u}{\partial x} + \frac{\partial u}{\partial y} = 0 \tag{1}$$

$$u\frac{\partial u}{\partial x} + v\frac{\partial u}{\partial y} = \frac{\nu}{(\lambda_2+1)}\left[\frac{\partial^2 u}{\partial y^2} + \lambda_1\left(u\frac{\partial^3 u}{\partial x \partial y^2} + v\frac{\partial^3 u}{\partial y^3} + \frac{\partial u}{\partial y}\frac{\partial^2 u}{\partial x \partial y} - \frac{\partial u}{\partial x}\frac{\partial^2 u}{\partial y^2}\right)\right] - \frac{\sigma B_0^2}{\rho} \tag{2}$$

$$\rho c_p\left(u\frac{\partial T}{\partial x} + v\frac{\partial T}{\partial y}\right) = k\frac{\partial^2 T}{\partial y^2} - \frac{\partial q_r}{\partial y} - Q_0(T - T_\infty) \tag{3}$$

$$u\frac{\partial C}{\partial x} + v\frac{\partial C}{\partial y} = D\frac{\partial^2 C}{\partial y^2} - K_{r*}(C - C_\infty) \tag{4}$$

where (u, v) represent the velocity components along the (x, y) axis, ρ represent the fluid's density, The kinematic velocity is represented by $\nu\left(=\frac{\mu}{\rho}\right)$. μ is the dynamic viscosity, B_0 represent the strength of the magnetic field, σ represent the conductivity of electricity, The ratio of relaxation and retardation time is represented by λ_2, and the relaxation time is represented by λ_1. The thermal conductivity represents by k, c_p represent the constant pressure specific heat, T represent the temperature,T_∞ represent the temperature constant far away from the sheet. Q_0 represent the coefficient of heat absorption/generation, The diffusion coefficient is represented by D. $K_r *$ represent the chemical reaction parameter, C_w represent the species concentration at the wall, and C_∞ represent the species concentrations far away from the wall.

2.1 Boundary Conditions

The boundary conditions that result from the previously stated assumptions are as follows

$$u = U_w(x) = cx;\ \ v = 0;\ \ T = T_\infty + A_1\left(\frac{x}{l}\right)^n = T_w;\ \ C = C_\infty + A_2\left(\frac{x}{l}\right)^n = C_w\ at\ y = 0 \tag{5}$$

$$u \to 0;\ u' \to 0;\ \ T \to T_\infty;\ \ C \to C_\infty\ as\ y \to \infty \tag{6}$$

The Rosseland approximation can be used to describe the radiative heat flux q_r [48, 49]

$$q_r = -\frac{4\sigma^*}{3k^*}\frac{\partial T^4}{\partial y} \tag{7}$$

The Stefan-Boltzman constant and the Rosseland mean absorption coefficient are represented by k^* and σ^*, respectively. By assuming T^4 expansion of the Taylor series and omitting higher-order terms, we get

$$T^4 \approx 4T_\infty^3 T - 3T_\infty^4 \tag{8}$$

Putting Eq. (7) in Eq. (8), we have

$$\begin{aligned} q_r &= -\frac{4\sigma^*}{3k^*}\frac{\partial}{\partial y}(4T_\infty^3 T - 3T_\infty^4) \\ q_r &= -\frac{16\sigma^*}{3k^*}\ T_\infty^3\frac{\partial T}{\partial y} \end{aligned} \tag{9}$$

Eq. (9) differentiate with respect to y, we have

$$\frac{\partial q_r}{\partial y} = -\frac{16\sigma^*}{3k^*}\ T_\infty^3\frac{\partial^2 T}{\partial y^2} \tag{10}$$

Substituting Eq. (10) in Eq. (3),

$$\rho c_p\left(u\frac{\partial T}{\partial x} + v\frac{\partial T}{\partial y}\right) = k\frac{\partial^2 T}{\partial y^2} + \frac{16\sigma^*}{3k^*}\ T_\infty^3\frac{\partial^2 T}{\partial y^2} - Q_0(T - T_\infty) \tag{11}$$

2.2 Similarity Transformation

$$u = cxf'(\xi), \quad \xi = \sqrt{\frac{c}{\nu}}y, \quad v = -\sqrt{c\nu}\, f(\xi), \ \theta(\xi) = \frac{T-T_\infty}{T_w-T_\infty}, \ \phi(\xi) = \frac{C-C_\infty}{C_w-C_\infty} \tag{12}$$

The similarity variable, dimensionless stream function, dimensionless temperature, and dimensionless concentration are represented by ξ, $f(\xi)$, $\theta(\xi)$ and $\phi(\xi)$, respectively. ψ is a stream function that is defined as $u = \frac{\partial \psi}{\partial y}$, $v = -\frac{\partial \psi}{\partial x}$.

2.3 Transformed problems

Therefore, after substitution of Eq. (5), (6) and (12) into Eq. (2) - (4), the governing equations in dimensionless form given by

$$\beta((f'')^2 - f\, f'^v) + f''' + (1+\lambda_2)(ff'' - f'^2 - Mf') = 0 \tag{13}$$

$$\left(\frac{3+4R}{3}\right)\theta'' + \Pr\,(f\theta' - mf'\theta + \gamma\theta = 0 \tag{14}$$

$$\phi'' + Sc\,(f\,\phi' - mf'\phi - Kr\phi) = 0 \tag{15}$$

Subject to

$$f(\xi) = 0,\ f'(\xi) = 1,\ \theta(\xi) = 1,\ \phi(\xi) = 1 \ \text{at}\ \xi = 0 \tag{16}$$

$$f'(\xi) = 0,\ f''(\xi) = 0,\ \theta(\xi) = 0, \phi(\xi) = 0 \ \text{as}\ \xi \to \infty \tag{17}$$

In the above equations, the Deborah number $\beta = \lambda_1 c$, the magnetic field parameter $M = \frac{\sigma B_0^2}{\rho c}$, the radiation parameter $R = \frac{16\sigma^* T_\infty^3}{k^* k}$, the Prandtl number $Pr = \frac{\rho c_p}{k}$, the heat sink/source parameter $\gamma = \frac{Q\nu}{\rho c_p}$, the Schmidt number $Sc = \frac{\nu}{D}$, and the chemical reaction parameter $Kr = \frac{Kr^*\delta^2}{\nu}$.

3. Method of Solution

In this study, to solve Eq. (13) - (15) subject to conditions Eq. (16) - (17), For the solution of the coupled nonlinear ordinary differential equation with boundary conditions, the Homotopy Analysis Method has been used to achieve an analytic approximation. It was first developed as HAM in 1992 and then modified HAM in 2004 by Liao [50]. A few authors apply the Homotopy analysis method to solve nonlinear equations in their research findings, and that shows the efficiency of HAM. The recent development shows the successful implementation of the HAM to get convergent approximate analytic solution for the non-Newtonian fluid flow analysis by Hayat *et al.,* [51], Qayyum *et al.,* [52] and Waqas *et al.,* [53]. To compute all the necessary solutions, we preferred to apply the Homotopy Analysis Method based on the BVPh2.0 Mathematica Package introduced by Liao [54]. The HAM is a more general method to validate strongly and weekly nonlinear problems because the HAM is independent of small or large parameters. It's also applicable throughout the problem domain and

isn't affected by rounding errors. With the idea of homotopy in topology, HAM offers us great freedom and independence to evaluate a superior solution from a family of alternatives.

We consider a collection of basis functions of the form: to explore this study of the Homotopy Analysis Method.

$$\left\{C_{m,n}\xi^n e^{mn} : m,n \geq 0\right\} \tag{18}$$

where $C_{m,n}$ coefficients to be determined.

The linear auxiliary operators L_f , L_θ and L_ϕ are selected in such a manner that all homogeneous equation solutions may be produced as linear combinations, as in Eq. (19).

$$L_f[f(\xi)] = 0, \;\; L_\theta[\theta(\xi)] = 0, \;\; L_\phi[\phi(\xi)] = 0 \tag{19}$$

As a result, we build all auxiliary linear operators systematically by examining higher order terms of the appropriate linear operator, as detailed in [55]. The auxiliary linear operator may be chosen in a following way:

$$L_f = \frac{d^3 f}{d\xi^3} - \frac{df}{d\xi} \tag{20}$$

$$L_\theta = \frac{d^2\theta}{d\xi^2} - \theta \tag{21}$$

$$L_\phi = \frac{d^2\phi}{d\xi^2} - \phi \tag{22}$$

Satisfying

$$L_f\left[C_1 + C_2 e^{\xi} + C_3 e^{-\xi}\right] = 0 \tag{23}$$

$$L_\theta\left[C_4 e^{\xi} + C_5 e^{-\xi}\right] = 0 \tag{24}$$

$$L_\phi\left[C_6 e^{\xi} + C_7 e^{-\xi}\right] = 0 \tag{25}$$

where $C_1, C_2, \ldots, C_7$ are the arbitrary constants to be determined from boundary conditions.

The initial estimates $f_0(\xi), \theta_0(\xi)$ and $\phi_0(\xi)$ are chosen to meet the criteria Eq. (16) - (17), and the co-efficient is calculated as follows

$$f_0(\xi) = 1 - e^{-\xi}, \;\; \theta_0(\xi) = e^{-\xi}, \;\; \phi_0(\xi) = e^{-\xi} \tag{26}$$

3.1 The Skin Friction, The Nusselt Number and The Sherwood Number

The skin friction coefficient, the local Nusselt number, and the Sherwood number are the physical parameters. Defined as follows

$$Re_x^{1/2} C_f = -\left(\frac{1}{1+\lambda_2}\right)(f''(0) + \beta f''(0)) \tag{27}$$

$$Nu_x Re_x^{-1/2} = -\left(\frac{3+4R}{3}\right)\theta'(0) \tag{28}$$

$$ShRe_x^{-1/2} = -\phi'(0) \tag{29}$$

4. Convergence Analysis

The convergence of the Homotopy Analysis Method is carried out on the solution to the proper selection of convergence-control parameters using the HAM-based Mathematica package BVPh2.0. Considering default values in built functions $\beta = 1.0$, $\lambda_2 = 0.1$, $M = 6.0$, $R = 0.1$, $Pr = 0.75, m = 2.0$, $\gamma = 0.1$, $Sc = 0.6$, and $Kr = 0.2$. The Homotopy analysis method convergence considers up to 40th order approximations throughout the study unless otherwise mentioned.

We can select convergence control parameters $\hbar_f, \hbar_\theta, \hbar_\phi$ as per our own choice despite linear operators, auxiliary functions, and initial guesses. Hence, these parameters are properly selected to have an accurate convergent series solution. Convergence control parameters associated with $\hbar$-curves are shown in Figure 2 and in the acceptable ranges for the auxiliary parameters, $\hbar$ curves are horizontal. The need of the HAM convergent solution for any value of the parameters from the following intervals provided in Eq. (30).

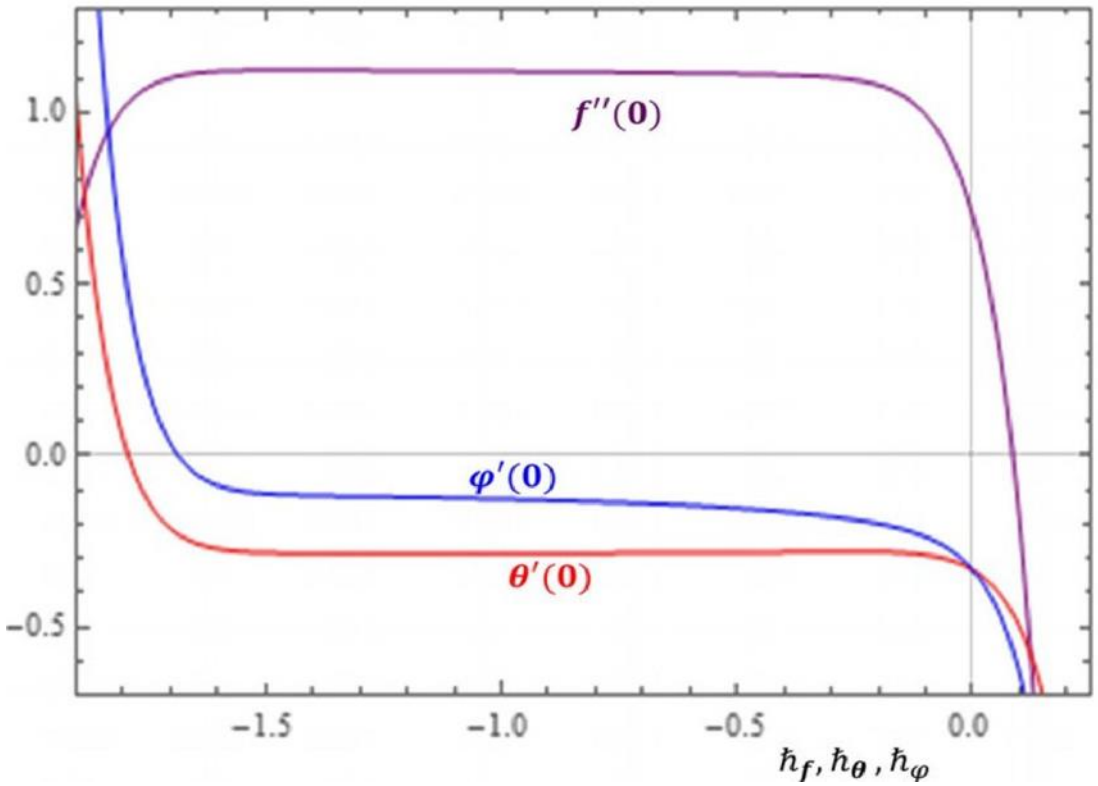

Fig. 2. h-curves

$$-0.4 < \hbar_f < -0.1, -1.5 < \hbar_\theta < -1.2, -1.6 < \hbar_\phi < -1.2 \tag{30}$$

The better values of the parameters can be found by comparing the convergent control parameters, but this is technically not effective. As a result, the optimum values of all parameters are determined by minimising squared-residual errors, which are specified and denoted by

$$\varepsilon_n^j \approx \frac{1}{N+1}\sum_{i=0}^{N}\left\{\aleph_j\left[\sum_{k=0}^{n}\varphi_k^j(\xi)_{\xi=i\Delta\xi}\right]\right\}^2 \tag{31}$$

The Mathematica package BVPh2.0 used to get the convergence control parameter optimal values and the values are

$$\hbar_f \approx -0.23, \hbar_\theta \approx -1.34, \hbar_\phi \approx -1.36$$

The evaluated boundary derivatives $-f''(0), -\theta'(0)$ and $-\phi'(0)$ and the required square residual error ε_f , ε_θ and ε_ϕ are shown in Table 1. The boundary derivatives $-f''(0)$ value convergent at 35^{th}, $-\theta'(0)$ convergent at 10^{th} and $-\phi'(0)$ convergent at 40^{th} order of approximation with an error tolerance of less than 0.00001. Thus, it is required to take the 40^{th} order of Homotopy Analysis Method approximation for evaluating the necessary results of the study and the individual square residual errors is decreasing as shown in Table 1. The total square residual error verses some order of HAM is shown in Figure 3 and since the order of the HAM approximation rises, the total average squared residual error reduces.

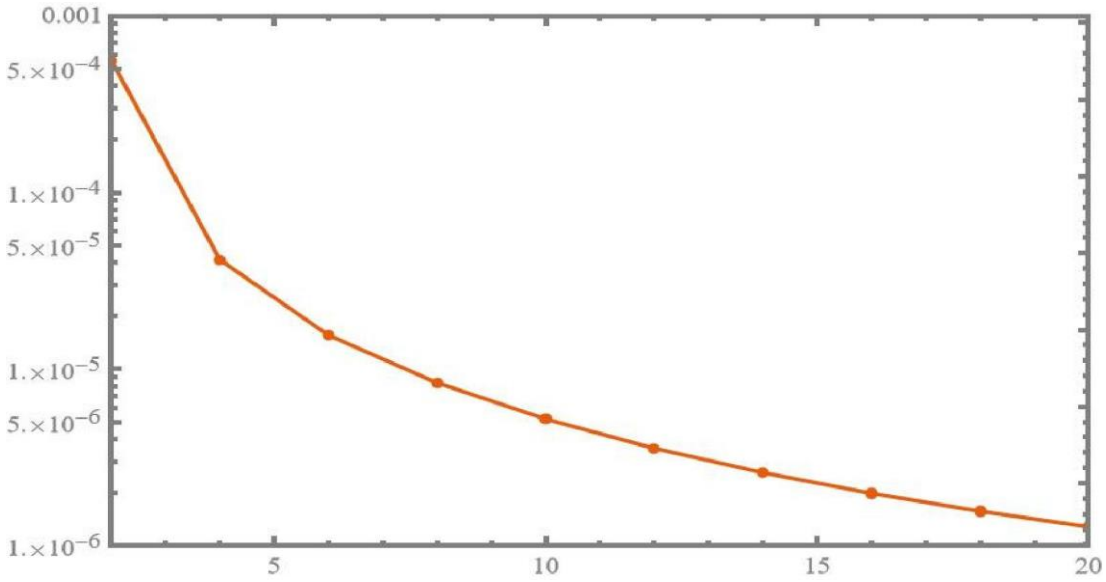

Fig. 3. Total squared residual errors against the order of approximation

Table 1
Convergence of solution with squared residual error for the Homotopy Analysis Method

Order	$-f''(0)$	$-\theta'(0)$	$\phi'(0)$	ε_f	ε_θ	ε_ϕ
05	1.944546	0.765700	0.282797	$7.14508 \cdot 10^{-3}$	$3.63876 \cdot 10^{-4}$	$2.06982 \cdot 10^{-5}$
10	1.961233	0.705828	0.866260	$5.65714 \cdot 10^{-6}$	$6.80690 \cdot 10^{-5}$	$2.44041 \cdot 10^{-7}$
15	1.962121	0.679724	0.865158	$1.75228 \cdot 10^{-7}$	$3.28037 \cdot 10^{-5}$	$1.65791 \cdot 10^{-8}$
20	1.962138	0.659440	0.864854	$2.51233 \cdot 10^{-9}$	$1.99295 \cdot 10^{-5}$	$4.96564 \cdot 10^{-10}$
25	1.962142	0.641616	0.864798	$2.27079 \cdot 10^{-10}$	$1.56129 \cdot 10^{-5}$	$5.02727 \cdot 10^{-11}$
30	1.962142	0.641674	0.864797	$7.75201 \cdot 10^{-12}$	$1.41153 \cdot 10^{-5}$	$2.09297 \cdot 10^{-12}$
35	1.962142	0.607311	0.864797	$1.20446 \cdot 10^{-12}$	$1.34849 \cdot 10^{-5}$	$2.52015 \cdot 10^{-13}$
40	1.962142	0.589227	0.864774	$7.10432 \cdot 10^{-14}$	$1.47251 \cdot 10^{-5}$	$1.23493 \cdot 10^{-14}$

5. Numerical Results and Discussion

This section illustrates the results of the electrical conduction magnetohydrodynamics Jeffrey Fluid across a Stretching Sheet of heat and mass transfer in a boundary layer flow in the presence of power-law concentration and temperature distributions and the effects of thermal radiation and chemical reaction with the heat source. The influence of the appropriate parameters on the distribution of velocity profile $f'(\eta)$, temperature profile $\theta(\eta)$, and nanoparticle concentration profile $\phi(\eta)$ are assessed using Jeffrey fluid depth analysis. Additionally, the coefficient of surface friction, Nusselt number, and Sherwood number maintain the stability of other parameters. We compared our findings for the rate of heat transfer with various values of m and Pr with that of Chen [56] to validate the accuracy of the current model. Table 2 shows that the comparisons are in excellent agreement. Increases in Pr and m have also been shown to enhance the local Nusselt number. Table 3 compares the local skin friction coefficient to Andersson *et al.,* [57] and Chen [58] for various magnetic parameter values. It is observed that when M increases, the skin friction coefficient decreases. Table 3 also shows that the comparisons are in excellent agreement.

The Mathematica package BVPh2.0 is applied to get solutions pictorially and numerically. The consequences of different physical parameters on fluid flow are observed From Figure 4 to Figure 20, the influence of various physical factors on fluid flow is shown.

Table 2
Validate the $-\theta'(0)$ for different values of Pr, m *when* $R = 0,\ \lambda = 0,\ \beta = 0,\ M = 0,\ Kr = 0$

	Chen [52]			Present Study		
Pr	$m=-2$	$m=0$	$m=2$	$m=-2$	$m=0$	$m=2$
0.72	-0.72000	0.46315	1.08853	0.719999	0.463145	1.088524
1	-1.00003	0.58199	1.33334	-1.00003	-0.581977	-1.333333
10	-10.0047	2.30796	4.79686	10.0047	2.30796	4.796859

Table 3
Validate the $-f''(0)$ for different values of M with $\lambda = 0,\ \beta = 0,\ M = 0$

M	Andersson *et al.,* [53]	Chen [54]	Present
0.0	1.0000	1.00000	1.000000
0.5	1.2250	1.22425	1.224745
1.0	1.4140	1.41421	1.414214
1.5	1.5810	1.58114	1.581139
2.0	1.7320	1.73205	1.732051

The magnetic field parameter M has a significant impact on the velocity profile $f'(\eta)$, as seen in Figure 4 for $\lambda_2 = 0.0$ as well as $\lambda_2 = 1.0$ and observe that when the velocity profile decreases, the magnetic field parameter increases because of the effect of Lorentz force and the resulting slowdown of the velocity profile. We also discovered that a rise in λ_2 induces a decrease in fluid boundary layer velocity. λ_2 is inversely related to non-Newtonian fluid retardant time. The fluid retardation time reduces as λ_2 rises, and the rushing of the fluid motion stops.

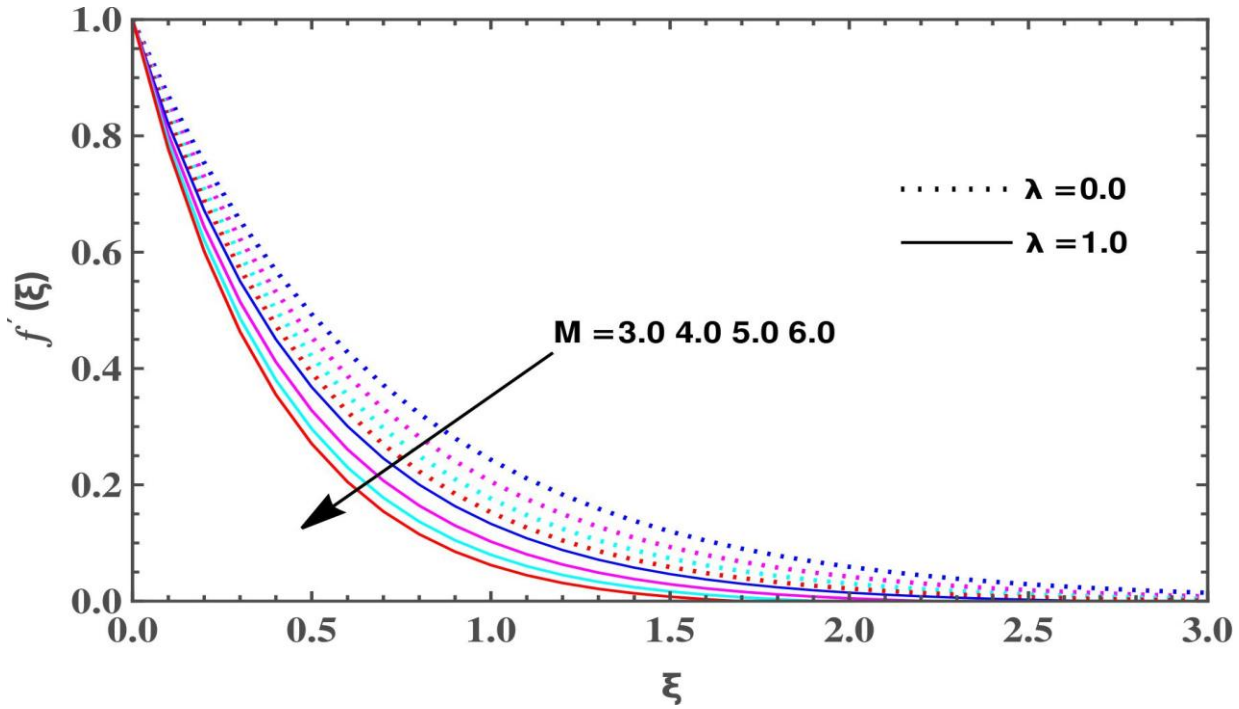

Fig. 4. The significant effect of different value of M on $f'(\xi)$ at $\beta = 1.0,\ Kr = 0.2,\ Sc = 0.6,\ R = 0.1,$ $\gamma = 0.1, m = 2.0,\ Pr = 0.75$

Figure 5 to 7 depicts the consequences of Deborah number β on the fluid velocity, temperature, and concentration profiles. The fluid's velocity profile increases when the β values increase, as seen in Figure 5. Based on empirical data, the Deborah number β is proportionally related to the rate of stretching of the sheet $\beta = \lambda_1 c$, with more significant fluid motion towards the surface of the sheet caused by the increased β. As fluid motion increases, the hydrodynamic boundary layer thickness rises. When β is growing, as in Figure 6, the temperature profile decreases, and the concentration profile likewise reduces. The number β is related to the time needed to halt motion, and this occurs anytime β rises, resulting in increasing retardation time. With a more extended retardation period, lower temperatures and thinner thermal boundary layer thicknesses are seen in Figure 7.

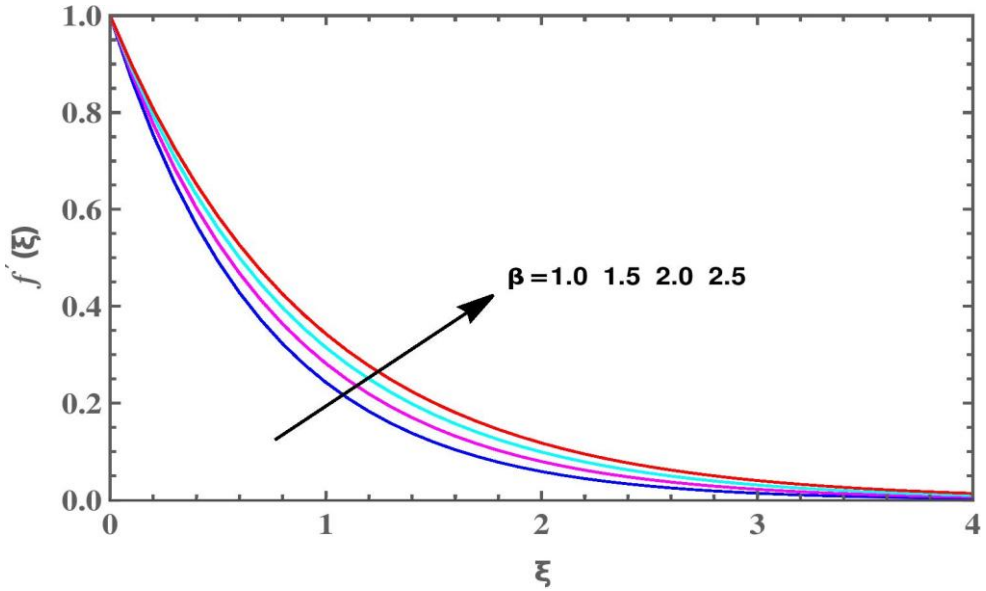

Fig. 5. The significant effect of different value of Deborah No. β on the $f'(\xi)$ at $Kr = 0.2,\ M = 1,\ Sc = 0.7, R = 0.1,\ \lambda_2 = 1.0,\ \gamma = 0.1,\ m = 2.0,\ Pr = 0.70$

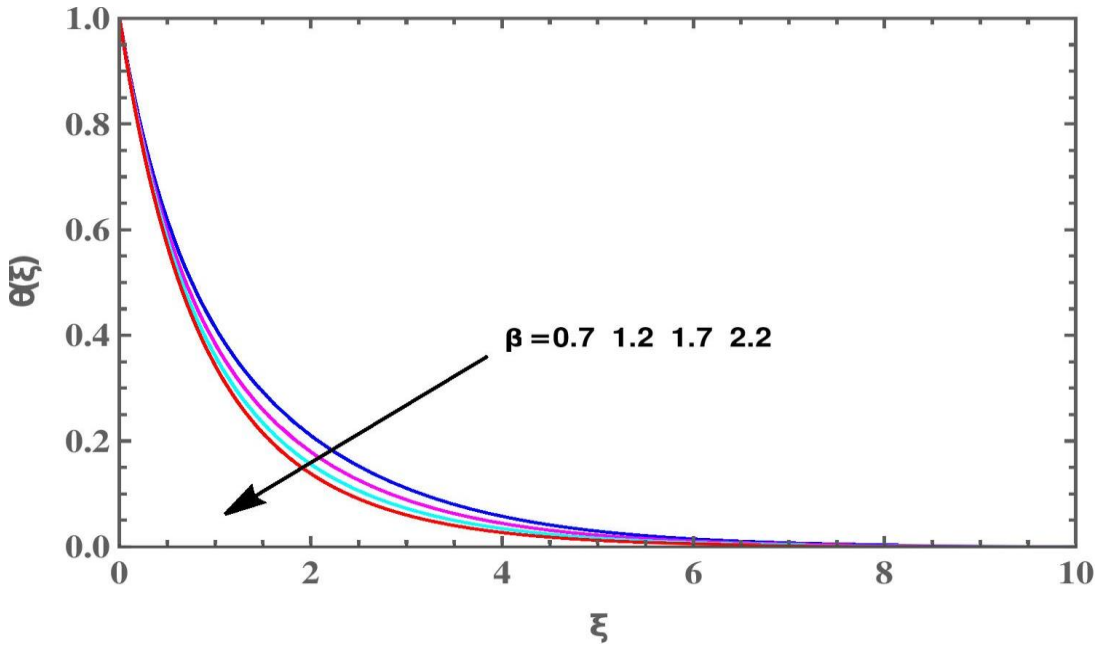

Fig. 6. The significant effect of different value of Deborah No. β on the $\theta(\xi)$ at $Pr = 1.0$, $Sc = 0.3, R = 0.1$, $\lambda_2 = 1.0$, $\gamma = 0.1$, $m = 2.0$, $M = 0.6$, $Kr = 0.2$

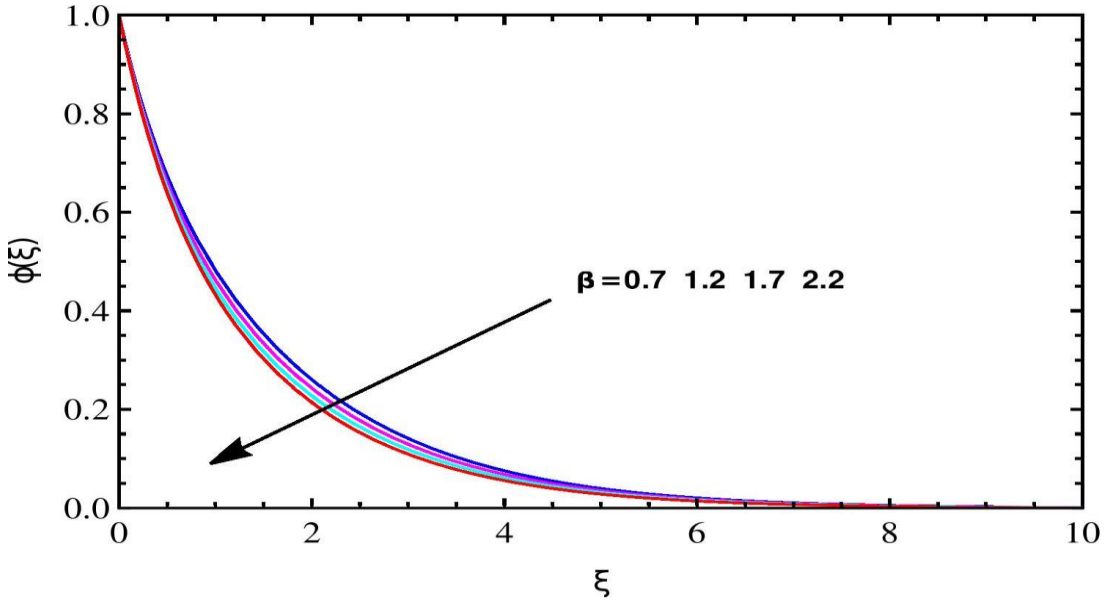

Fig. 7. The significant effect of different value of Deborah No. β on the $\phi(\xi)$ at $Pr = 0.70$, $Sc = 0.6$, $R = 0.2$, $\lambda_2 = 1.0$, $\gamma = 0.1$, $m = 2.0$, $M = 2.0$, $Kr = 0.2$

As seen in Figure 8, the Deborah numbers β, λ_2, and R have a significant effect on the temperature profile. This is because the temperature distribution becomes greater as R rises. Thermal radiation rises with increasing thermal boundary layer thickness. Consequently, the cooling process proceeds as quickly as feasible to reduce radiation. As a result of bulky fluid movements that affect the thickness of the thermal boundary layer, the temperature profile increases somewhat as the Deborah number β increases towards the sheet surface. As a result of this, the temperature profile has no effect on the β or the λ_2 values within a short distance of the sheet surface ($\eta = 0$).

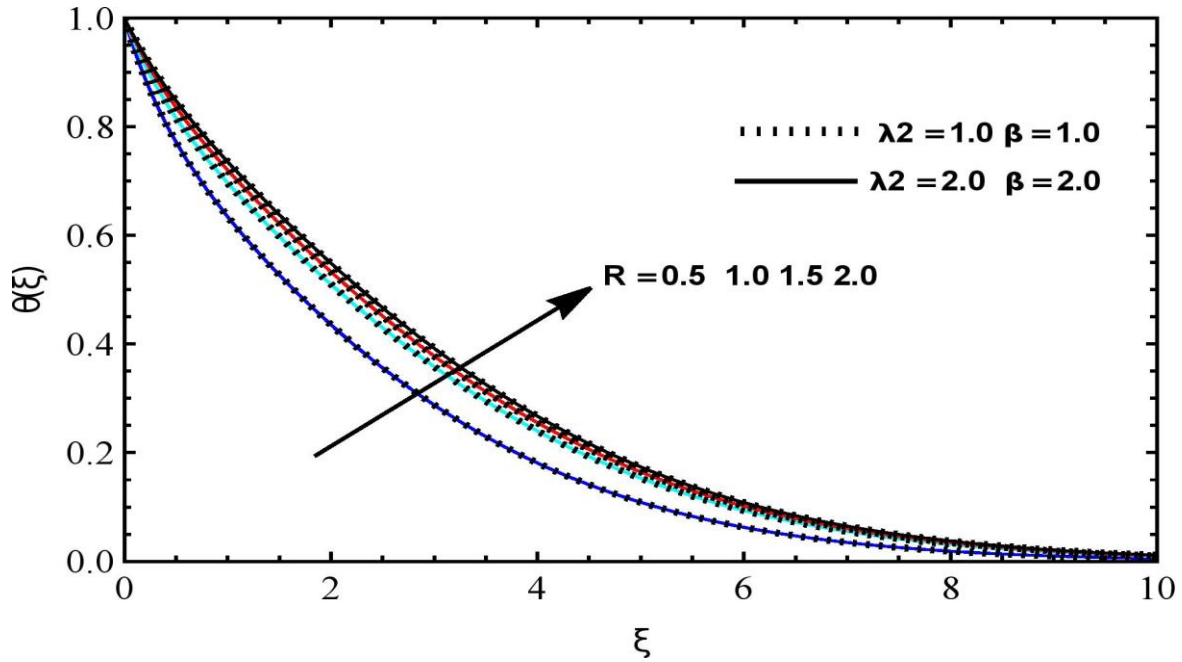

Fig. 8. The significant effect of different values of R, λ_2 and β on $\theta(\xi)$ at $Pr = 1.0,\ Sc = 0.6,\ M = 5.0, \gamma = 0.1,\ m = 2.0,\ Kr = 0.2$

The impacts of magnetic field settings on these data points are demonstrated in Figure 9 by looking at the temperature profiles. The temperature profile grows as the value of M increases. The temperature profile rises as the magnetic field approaches the retardant velocity field. The flow properties may be influenced by using a magnetic field.

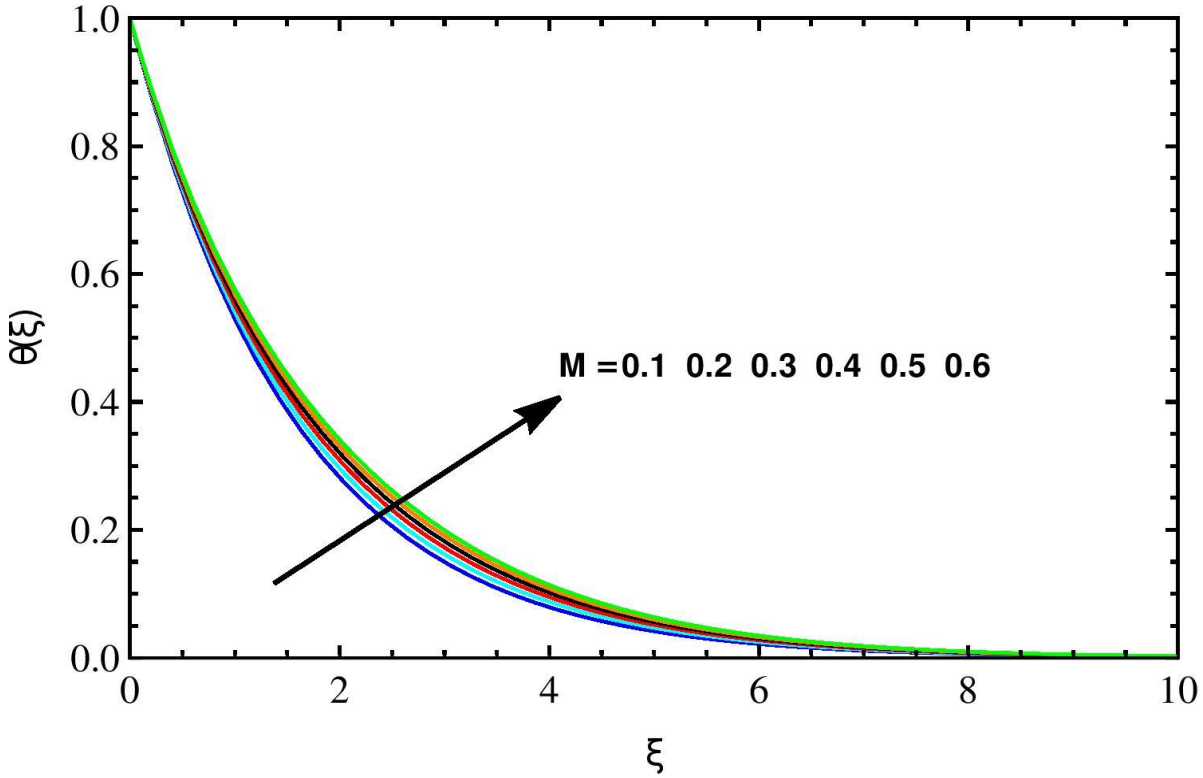

Fig. 9. The significant effect of different values of M on $\theta(\xi)$ at $Pr = 0.9,\ Sc = 0.6, \lambda_2 = 0.5,\ \beta = 1.9,\ R = 0.2,\ m = 0.9,\ \gamma = 0.3,\ Kr = 0.1$

The results are shown in Figure 10, which shows the impact of the Prandtl number Pr on the temperature profile. The temperature profile falls as the Prandtl number Pr rises. Because of Pr on thermal diffusivity, the temperature profile tends to be retarding. The higher Prandtl number, measured using Prandtl numbers, correlates with reduced thermal diffusivity, reducing temperatures and thins the thermal boundary layer.

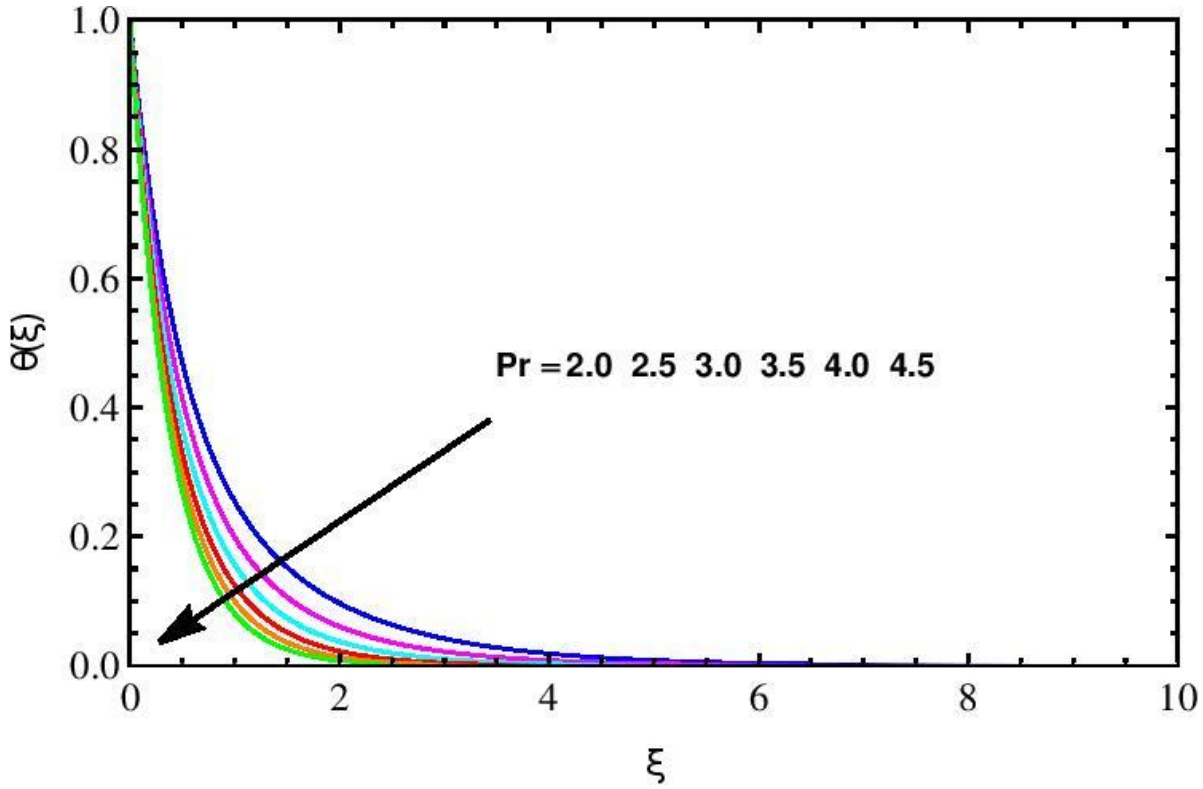

Fig. 10. The significant effect of different values of Prandtl number Pr on $\theta(\xi)$ at $\lambda_2 = 2.0,\ Sc = 0.8,$ $\beta = 2.0,\ M = 0.7,\ R = 0.4,\ m = 3.0,\ \gamma = 0.2,\ Kr = 0.3$

A chemically reacted parameter Kr impacts the concentration profile and ratio of relation and retard times, as shown in Figure 11. The concentration profile is similarly affected by $\lambda_2 = 0.1$ and 1.1. $\phi(\eta)$ drops as Kr and λ_2 increase. As chemical reaction parameters rise, the species concentration and border layer physically decrease. Figure 12 shows the effect of heat sink and heat source parameters $\gamma > 0$ and $\gamma < 0$ on temperature profiles. As a result of the heat source, the fluid temperature is rising. The boundary layer produces energy because the heat-source increases, which raises the temperature of the fluid and causes the fluid to become hotter. Still, since the fluid loses heat to the heat sink, its temperature is also dropping. The fluid temperature drops because heat sinking in the boundary layer absorbs heat. Another piece of information requires the observer that the heat sink is essential for the efficiency of the cooling of starched sheets.

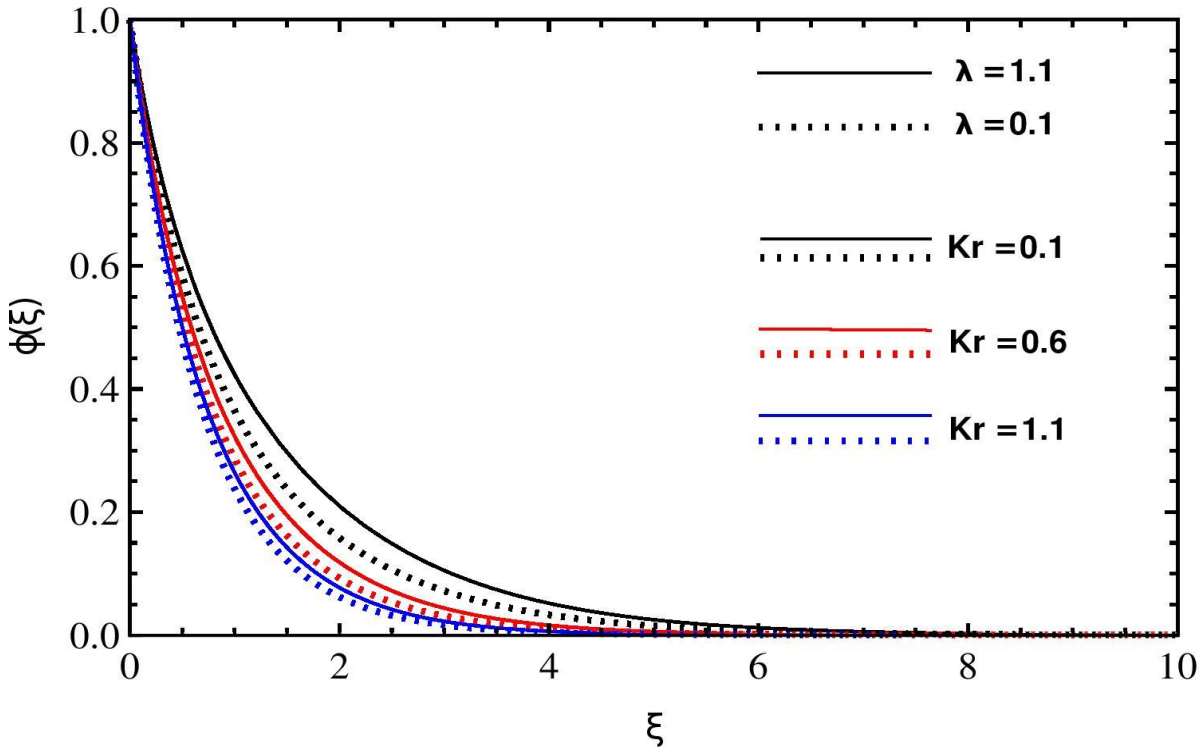

Fig. 11. The significant effect of different values of Kr with $\lambda_2 = 0.1$ and 1.1 on $\phi(\xi)$ at $Sc = 0.80$, $M = 2.1,\ m = 2.1,\ Pr = 0.80,\ \gamma = 0.2,\ R = 0.2,\ \beta = 1.1$

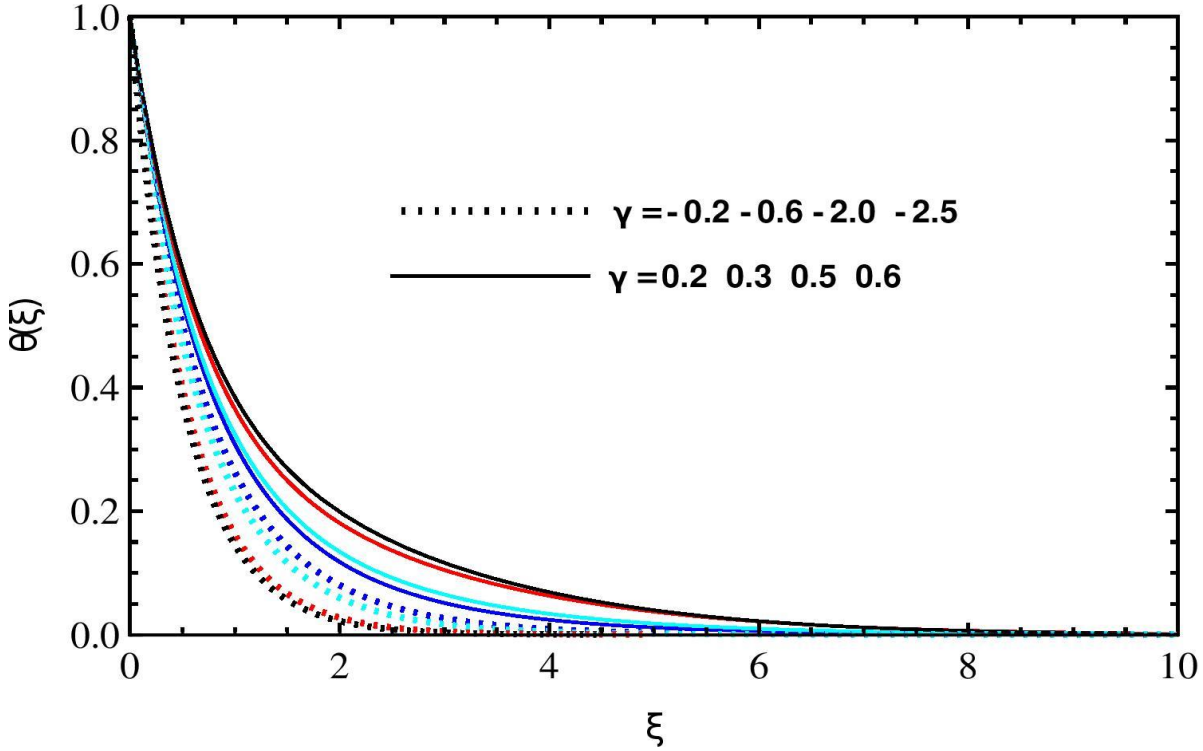

Fig. 12. The significant influence of various values of heat source or sink parameter γ on $\theta(\xi)$ at $\lambda_2 = 0.3,\ Sc = 0.4,\ \beta = 2.0,\ M = 0.5,\ R = 0.3, m = 3.0,\ Pr = 1.0,\ Kr = 0.3$

Figure 13 indicates the impact of Schmidt No. (Sc) on concentration profiles. The molecular diffusion is decreasing as Schmidt No. Sc increases. Thus, when the Schmidt No. (Sc) is small, the concentration profile is higher. Similarly, the concentration profile is lower for larger Schmidt No.

(Sc). So, the concentration profile decreases as Schmidt No. (Sc) increases and retardants in the fluid velocity.

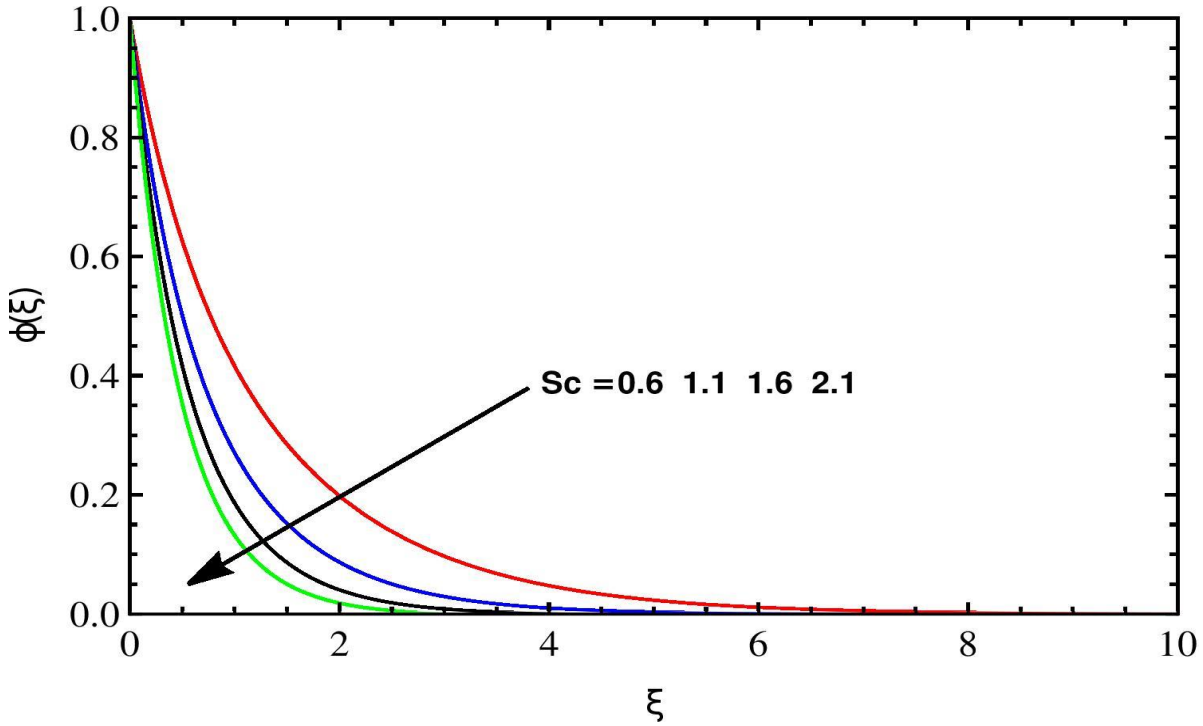

Fig. 13. The significant effect of different values of Sc on $\phi(\xi)$ at $Pr = 0.80, \gamma = 0.2,\ \lambda_2 = 1.1,\ \beta = 1.1,\ R = 0.2,\ m = 2.1,\ Kr = 0.3,\ M = 1.1$

In Figure 14, one can see how the surface temperature parameter (m) influences the temperature distribution. When the value of m rises, the temperature profile decreases because the sheet stretches as the free stream temperature is lower than the sheet's temperature. More specifically, $T_\infty < T_w$. Because temperature distribution is falling and the boundary layer thickness is decreasing, ξ rises. The concentration profiles decrease as the wall concentration parameter m rises shown in Figure 15.

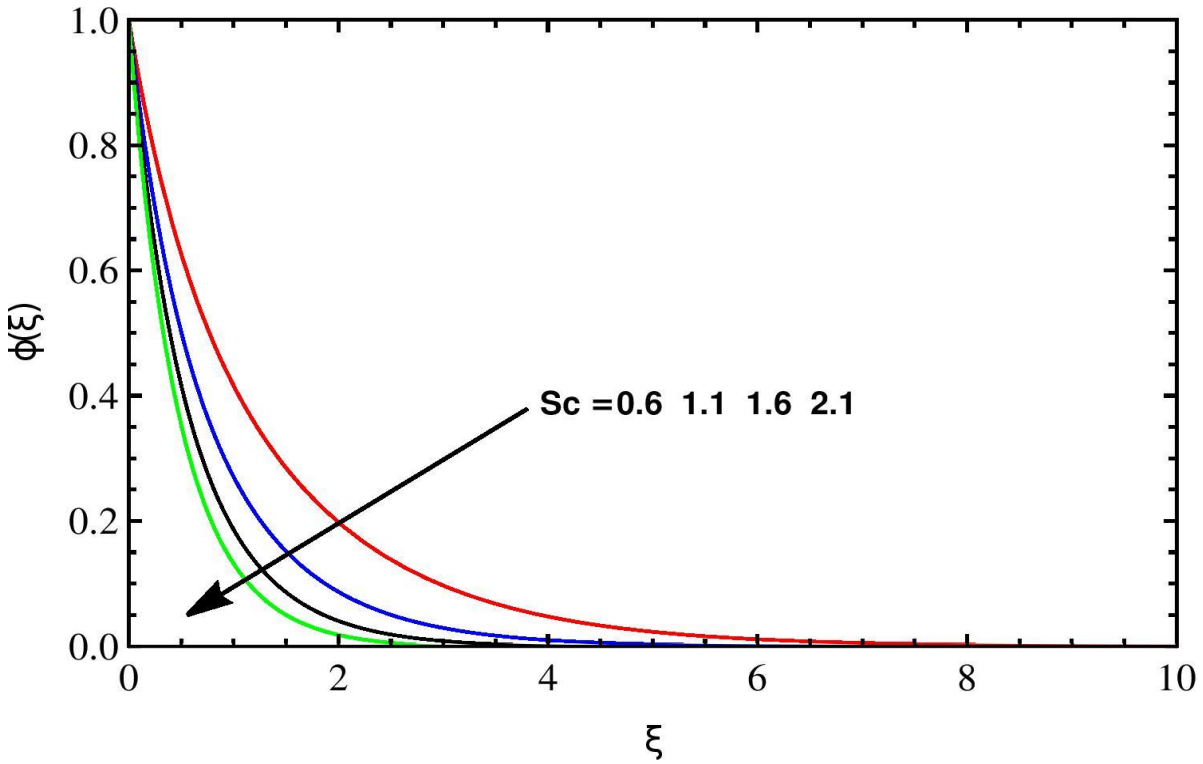

Fig. 14. The significant effect of different values of surface temperature parameter m on $\theta(\xi)$ at $\lambda_2 = 1.1, Sc = 0.8, \beta = 1.1, M = 0.7, R = 0.3, \gamma = 0.2, Pr = 1.1, Kr = 0.3$

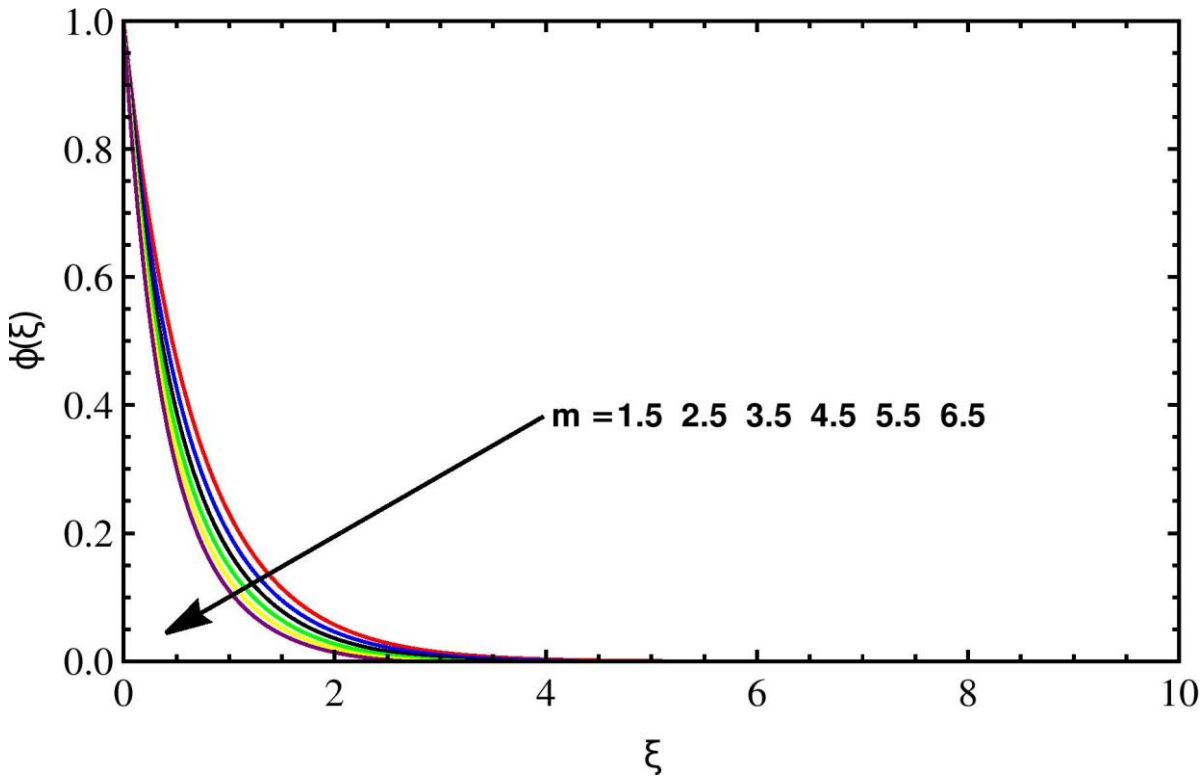

Fig. 15. The significant influence of various values of surface temperature parameter m on $\phi(\xi)$ at $Pr = 1.20, \gamma = 0.6,\ \lambda_2 = 1.5,\ \beta = 1.5,\ R = 0.5,\ Sc = 1.2,\ Kr = 0.7,\ M = 1.5$

In Figure 16 and Figure 17 shows considerable change in the skin-friction coefficient and the Nusselt number with λ_2 for different values of β. It has been noticed that when β increases, the skin-friction coefficient reduces. This is because increasing β causes more fluid particles to move into the

boundary layer, particularly near the sheet surface. Consequently, the velocity boundary layer thickness decreases, resulting in reduced skin-friction coefficient values. In comparison, when λ_2 grows, so does the skin friction coefficient. Physically, when λ_2 is increasing then the non-Newtonian character of the fluid increases and so, At the sheet surface velocity of the fluid reduces. As a result, the thickness of the hydrodynamic boundary layer rises, causing the local skin friction coefficient to rise. It's also worth noting that the fluctuation of Nusselt number with and is precisely opposite that of skin friction. This is because increasing contributes to the thickness of the thermal boundary layer, causing the Nusselt number to decrease.

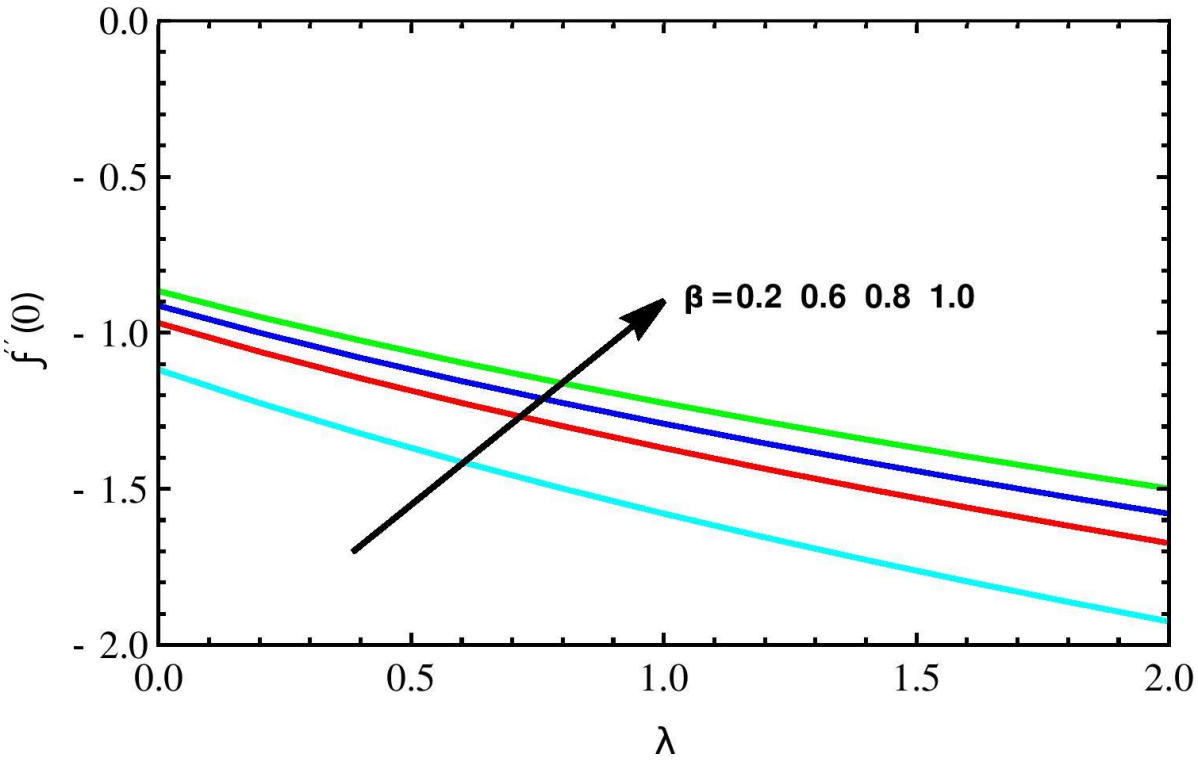

Fig. 16. Variation of skin friction coefficient versus λ_2 has a considerable influence for various values of β at $Pr = 0.72,\ \gamma = 0.1,\ R = 0.2,\ Sc = 0.69,\ Kr = 0.2,\ M = 0.5,\ m = 2.0$

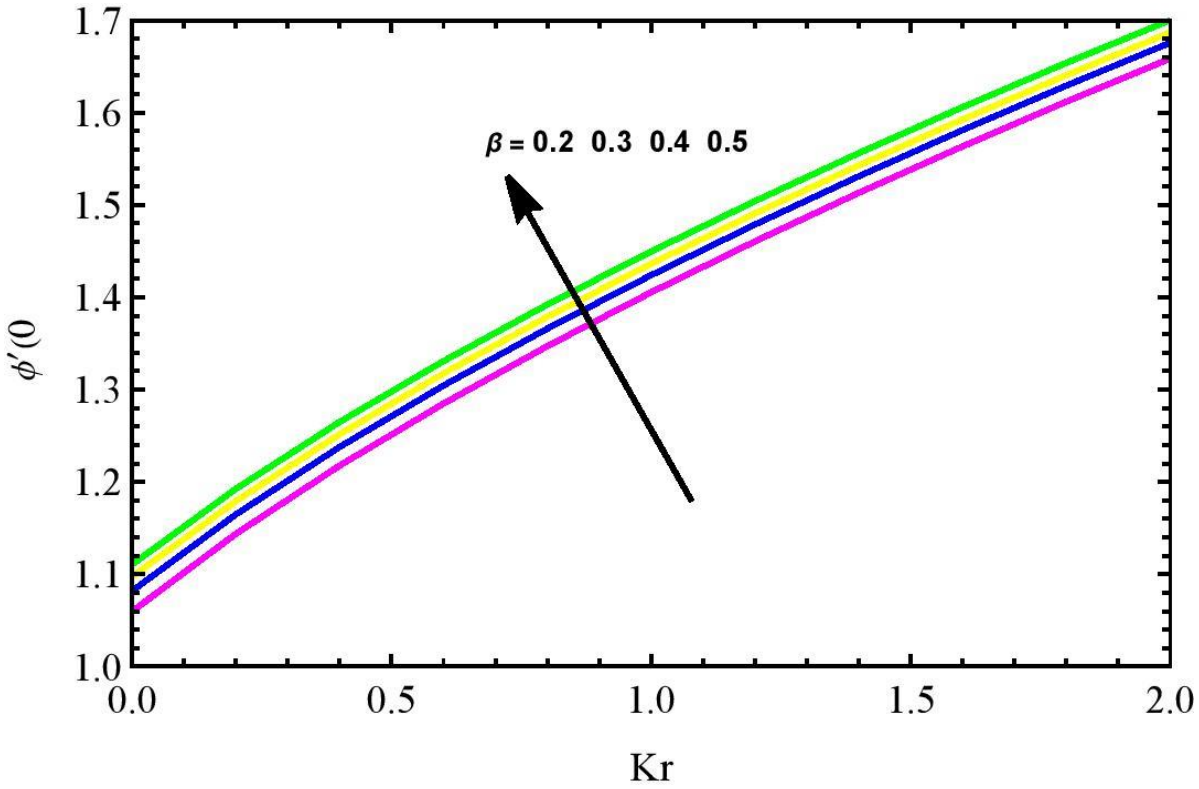

Fig. 17. Variation of the Nusselt number versus λ_2 has a considerable influence for various values of β at $Pr = 0.40, \gamma = 3.0,\ R = 0.70,\ Sc = 0.71,\ M = 0.5,\ m = 2.0,\ Kr = 0.1$

In Figure 18 and Figure 19 shows the considerable change in the local Nusselt and Sherwood numbers, as well as the Prandtl number Pr, for different values of R and β. Note that the Nusselt and Sherwood numbers are growing with rising values of R, Pr and β.

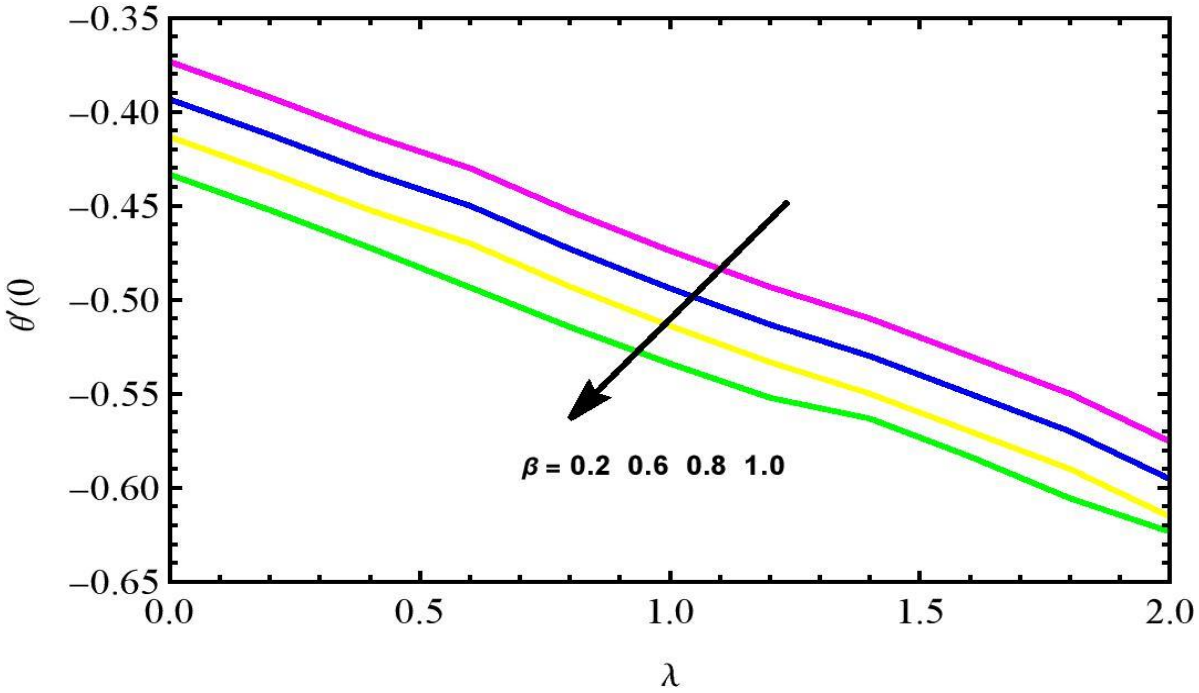

Fig. 18. Variations of the Sherwood number versus Kr has a considerable influence for various values of β at $Pr = 0.40,\ \lambda_2 = 0.1,\ \gamma = 3.0, R = 0.70,\ Sc = 0.71, M = 0.5, m = 2.0$

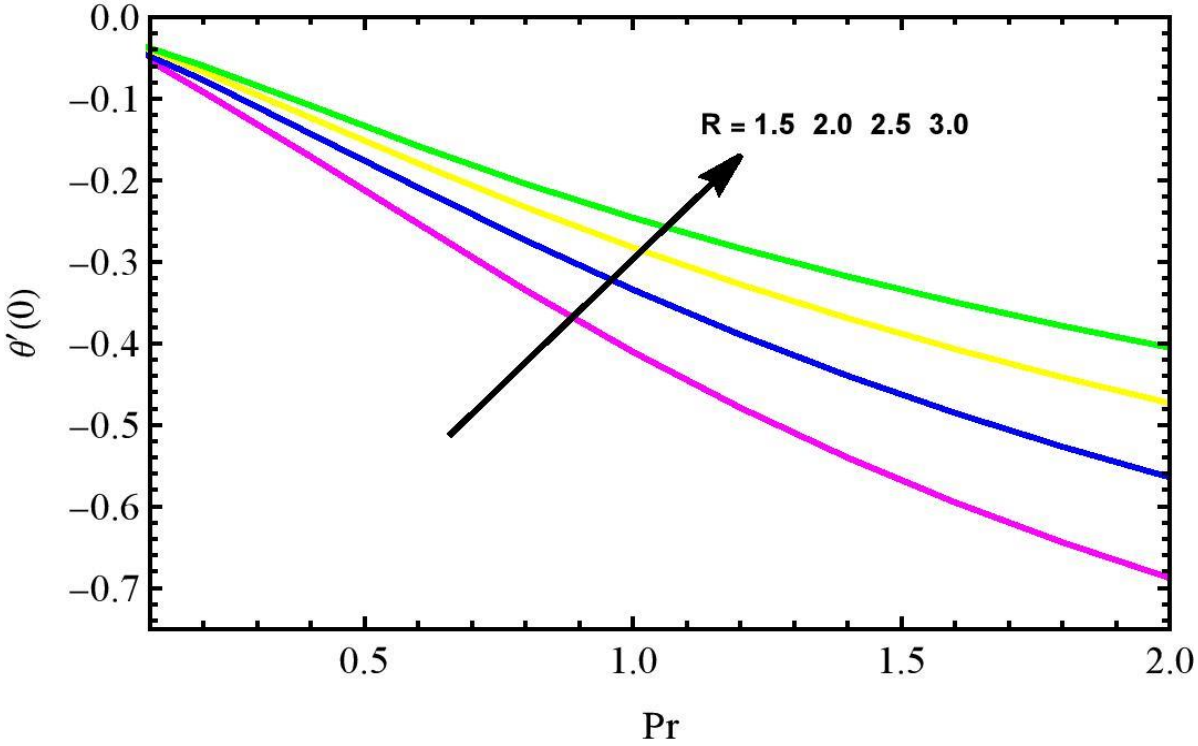

Fig. 19. Variations of Nusselt number versus Pr has a considerable influence for various values of R at $\beta = 0.2, \gamma = 3.5,\ \lambda_2 = 0.70,\ Sc = 0.750,\ M = 0.6, m = 1.5, Kr = 0.2$

It is observed from Figure 20, When parameter β raises, then the local skin friction co-efficient $f''(0)$ dropping. Increasing β means a reduction in the yield stress of the Jeffrey fluid and a rise in the value of plastic dynamic viscosity, Physically, which generates resistance in fluid flow.

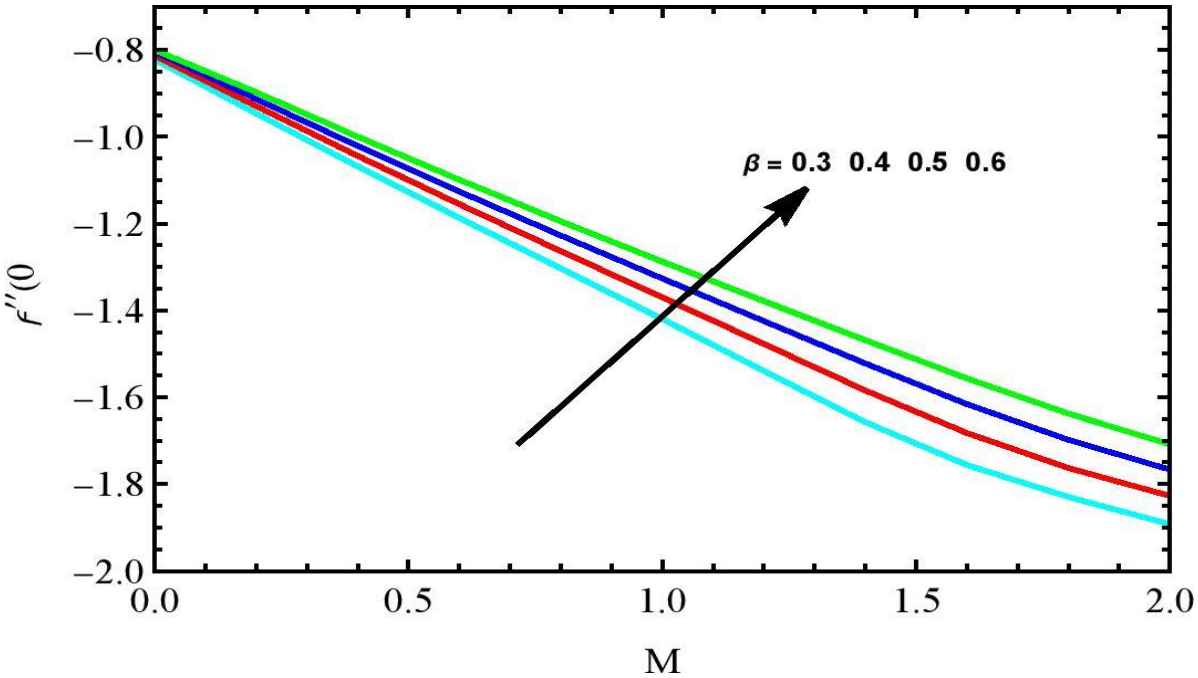

Fig. 20. Variations of Nusselt number versus Pr has a considerable influence for various values of R at $\beta = 0.2, \gamma = 3.5,\ \lambda_2 = 0.70,\ Sc = 0.750,\ M = 0.6, m = 1.5,\ Kr = 0.2$

From Table 4, Skin friction, Nusselt number and Sherwood number decrease with an increase in λ_2 and γ, whereas they increase with the rise in β and Kr. Skin friction decreases with an increase in R and m, whereas it increases with M. Nusselt number increases with R and m. The Sherwood number decreases with an increase in M and R, rising with an m increase.

Table 4
Data of Skin friction Coefficient, Nusselt Number and Sherwood Number at $Sc = 0.6$ & $Pr = 0.75$

λ_2	β	M	R	m	γ	Kr	$-\left(\frac{1+\beta}{1+\lambda_2}\right)f''(0)$	$-\left(\frac{3+4R}{3}\right)\theta'(0)$	$-\phi'(0)$
0.1	1.0	6.0	0.1	2.0	0.1	0.2	3.53553872	0.86779287	0.88279750
0.2							3.37095674	0.85182385	0.87220164
0.3							3.22483390	0.83757187	0.86269696
	2.0						4.00596187	0.91270248	0.91266392
	3.0						4.63816606	0.96871467	0.94971020
		7.0					4.95428167	0.94261434	0.93246624
		8.0					5.24767912	0.91971431	0.91730732
			0.2				5.24763505	0.94965825	0.91730615
			0.3				5.24736016	0.96983025	0.91729920
				3.0			5.24738760	1.25526117	1.10131831
				4.0			5.24718780	1.50194359	1.27103524
					0.2		5.24701994	1.44290846	1.27102429
					0.3		5.24683224	1.37893207	1.27101237
						0.3	5.24686299	1.37893781	1.30399390
						0.4	5.24688653	1.37894223	1.33531839

6. Conclusion

The present work deals with two-dimensional boundary layer magneto-hydrodynamic (MHD) flow and heat transfer of a Jeffrey fluid over a stretching sheet with thermal radiation and chemical reaction power-law form of temperature and concentration are numerically discussed in this article. Numerical results are tabulated for the skin-friction coefficient and the local Nusselt number to reveal the tendency of the solutions. Representative temperature profiles and the heat transfer parameter are observed for various controlling parameters. It can be drawn from the present results that the magnetic field increases the fluid temperature, raises the sheet surface temperature, and thickens the thermal boundary layer. The important points of present analysis are

i. As Deborah number β rises, the rate of heat transmission increases, and skin friction decreases.
ii. The temperature increases in the thermal boundary layer as the effect of the thermal radiation but notice that the opposite effect on temperature is observed when Prandtl number (Pr) increases.
iii. The velocity of the fluid is increasing within the boundary layer when Deborah number β increases, whereas the velocity of the fluid is decreasing when ratio of relaxation and retardation time λ_2 increases.
iv. When chemical reaction parameters increase, the concentration profile is decreasing.
v. The impact of magnetic field is to slowdown the velocity of flow field to a significant amount throughout the boundary layer.
vi. According to the current findings, Choosing Deborah number $\beta = 0$, one can be recovered the case of Newtonian fluid. Additional current work may be extended to significant

subtopics of non-Newtonian fluids likes of Oldroyd-B fluid, Maxwell fluid, and Eyring-Powell fluid.

Acknowledgement
This research was not funded by any grant.

References
[1] Sakiadis, B.C. "Boundary-layer equations for two-dimensional and axisymmetric flow." *American Institute of Chemical Engineering 7*, no. 1 (1961) : 26–28. https://doi.org/10.1002/aic.690070108
[2] Crane, L.J. "Flow past a stretching plate." *Journal of Applied Mathematics and Physics (ZAMP)* 21 (1970): 645–647. https://doi.org/10.1007/BF01587695
[3] Merkin, J.H. and Kumaran, V. "The unsteady MHD boundary-layer flowon a shrinking sheet." *European Journal of Mechanics - B/Fluids* 29, no. 5 (2010) : 357-363. https://doi.org/10.1016/j.euromechflu.2010.03.006
[4] Sheikholeslami, M., Gorji-Bandpay, M. and Ganji, D.D. "Magnetic field effects on natural convection around a horizontal circular cylinder inside a square enclosure filled with nano-fluid." *International Communications in Heat and Mass Transfer* 39, no. 7 (2012): 978–986. https://doi.org/10.1016/j.icheatmasstransfer.2012.05.020
[5] Ashorynejad, R.R, Sheikholeslami, M., Pop, I., Ganji, D.D. "Nanofluid flow and heat transfer due to a stretching cylinder in the presence of magnetic field." *Heat & Mass Tran* 49 (2013): 427–436. https://doi.org/10.1007/s00231-012-1087-6
[6] Cortell, R. "Fluid flow and radiative nonlinear heat transfer over a stretching sheet." *Journal of King Saud University - Science*, 26, no. 2 (2014) : 161-167. https://doi.org/10.1016/j.jksus.2013.08.004
[7] Akbar, N.S, Khan Z.H., Haq, R. and Nadeem, D. "Dual solutions in MHD stagnation-point flow of Prandtl fluid impinging on shrinking sheet." *Applied Mathematics & Mechanics* 35, no. 2 (2014): 813–820. https://doi.org/10.1007/s10483-014-1836-9
[8] Nourazar, S.S., Hatami, M., Ganji, D.D. and Khazayinejad, M. "Thermal-Flow Boundary Layer Analysis of Nano-fluid over a porous stretching Cylinder under the Magnetic Field Effect." *Power Technology* 317 (2017) : 310–319. https://doi.org/10.1016/j.powtec.2017.05.010
[9] Nagendramma, V., Leelarathnam, A., Raju, C.S.K, Shehzad S.A. and Hussain, T. "Doubly stratified MHD tangent hyperbolic nanofluid flow due to permeable stretched cylinder." *Results in Physics* 9 (2018) : 23–32. https://doi.org/10.1016/j.rinp.2018.02.019
[10] Khan, M., Salahuddin, T., Tanveer, A., Malik, M.Y. and Hussain, A. "Change in internal energy of thermal diffusion stagnation point Maxwell nano-fluid flow along with solar radiation and thermal conductivity." *Chinese Journal of Chemical Engineering* 27, no. 10 (2019) : 2352–2358. https://doi.org/10.1016/j.cjche.2018.12.023
[11] Waqas, M., Shehzad, S.A., Hayat, T., Khan, M.L. and Alsaedid, A. "Simulation of magneto-hydrodynamics and radiative heat transportation in convectively heated stratified flow of Jeffrey nanofluid." *Journal of Physics and Chemistry of Solids* 133 (2019): 45–51. https://doi.org/10.1016/j.jpcs.2019.03.031
[12] Dawar, A., Wakif, A., Saeed, A., Shah, Z., Muhammad, T. and Kumam, P., "Significance of Lorentz forces on Jeffrey nanofluid flows over a convectively heated flat surface featured by multiple velocity slips and dual stretching constraint: a homotopy analysis approach." *Journal of Computational Design and Engineering* 9 (2022) : 564- 582, https://doi.org/10.1093/jcde/qwac019
[13] Qasim, M. "Heat and mass transfer in a Jeffrey fluid over a stretching sheet with heat source/sink." *Alexandria Engineering Journal* 52, no. 4 (2013): 571-575. https://doi.org/10.1016/j.aej.2013.08.004.
[14] Nadeem, S., Rashid, M. and Akbar, N.S. "Optimized analytical solution for oblique flow of a Casson-nano fluid with convective boundary conditions." *International Journal of Thermal Sciences* 78 (2014) : 90–100. https://doi.org/10.1016/j.ijthermalsci.2013.12.001
[15] Shehzad, S.A., Alsaedi, A., Hayat, T. and Alhuthali, M.S. "Thermophoresis particle deposition in mixed convection three-dimensional radiative flow of an Oldroyd-B fluid." *Journal of the Taiwan Institute of Chemical Engineers* 45, no. 3 (2014) : 787–794. https://doi.org/10.1016/j.jtice.2013.08.022
[16] Akbar, N.S., Ebaid, A. and Khan, Z.H. "Numerical analysis of magnetic field effects on Eyring-Powell fluid flow towards a stretching sheet." *Journal of Magnetism and Magnetic Materials* 382 (2015) : 355-358. https://doi.org/10.1016/j.jmmm.2015.01.088
[17] Ashraf, M.B., Hayat, T., Alsaedi, A. and Shehzad , S.A. "Soret and Dufour effects on the mixed convection flow of an Oldroyd-B fluid with convective boundary conditions." *Results in Physics* 6 (2016): 917–924. https://doi.org/10.1016/j.rinp.2016.11.009

[18] Ahmad, K. and Ishak, A. "Magneto-hydrodynamic (MHD) Jeffrey fluid over a stretching vertical surface in a porous medium." *Propulsion and Power Research* 6, no. 4 (2017) : 269–276. https://doi.org/10.1016/j.jppr.2017.11.007

[19] Ganesh, N.V., Chamkha, A.J., Al-Mdallal, Q.M. and Kameswaran, P.K . "Magneto-Marangoni nano-boundary layer flow of water and ethylene glycol based $\gamma\ Al_2\ O_3$ nano-fluids with non-linear thermal radiation effects." *Case Studies in Thermal Engineering* 12 (2018) : 340–348. https://doi.org/10.1016/j.csite.2018.04.019

[20] Patel, Manoj R., and Jigisha U. Pandya. "Numerical study of a one and two-dimensional heat flow using finite volume." *Materials Today: Proceedings* 51 (2022): 48-57. https://doi.org/10.1016/j.matpr.2021.04.413

[21] Patel, Manoj R., and Jigisha U. Pandya. "A research study on unsteady state convection diffusion flow with adoption of the finite volume technique." *Journal of Applied Mathematics and Computational Mechanics* 20, no. 4 (2021): 65-76. https://doi.org/10.17512/jamcm.2021.4.06

[22] Naz, S., Gulzar, M.M., and Waqas, M. "Numerical modelling and analysis of non-Newtonian nano-fluid featuring activation energy." *Applied Nanoscience* 10 (2020): 3183–3192. https://doi.org/10.1007/s13204-019-01145-8

[23] Mittal, A.S. and Patel, H.R. "Influence of thermophoresis and Brownian motion on mixed convection two dimensional MHD Casson fluid flow with non-linear radiation and heat generation." *Physica A* 537 (2020): 122710 https://doi.org/10.1016/j.physa.2019.122710

[24] Cortell, R. "MHD (magneto-hydrodynamic) flow and radiative nonlinear heat transfer of a viscoelastic fluid over a stretching sheet with heat generation/absorption." *Energy* 74 (2014): 896–905. https://doi.org/10.1016/j.energy.2014.07.069

[25] Bhatti, M.M. and Zeeshan, A. "Analytic study of heat transfer with variable viscosity on solid particle motion in dusty Jeffery fluid." *Modern Physics Letters B* 30 (2016): 1650196. https://doi.org/10.1142/S0217984916501967

[26] Ramesh, K. "Effects of viscous dissipation and Joule heating on the Couette and Poiseuille flows of a Jeffrey fluid with slip boundary conditions." *Propulsion and Power Research* 7 no. 4 (2018): 329–341. https://doi.org/10.1016/j.jppr.2018.11.008

[27] Kahshan, M., Lu, D. and Siddiqui, A.M. "A Jeffrey fluid model for a porous walled channel: application to flat plate dialyzer." *Scientific Reports* 9 (2019): 15879. https://doi.org/10.1038/s41598-019-52346-8

[28] Khan, Ansab Azam, Khairy Zaimi, Suliadi Firdaus Sufahani, and Mohammad Ferdows. "MHD flow and heat transfer of double stratified micropolar fluid over a vertical permeable shrinking/stretching sheet with chemical reaction and heat source." *Journal of Advanced Research in Applied Sciences and Engineering Technology* 21, no. 1 (2020): 1-14. https://doi.org/10.37934/araset.21.1.114

[29] Shehzad, S.A., Abdullah, Z., Alsaedi, A. "Thermally radiative three-dimensional flow of Jeffrey nanofluid with internal heat generation and magnetic field." *Journal of Magnetism and Magnetic Materials* 397 (2016): 108–114. https://doi.org/10.1016/j.jmmm.2015.07.057

[30] Venkateswarlu, B, Narayana, P.V.S. "Chemical reaction and radiation absorption effects on the flow and heat transfer of a nanofluid in a rotating system." *Applied Nanoscience* 5 (2015): 351-360. https://doi.org/10.1007/s13204-014-0324-3

[31] Irfan, M., Khan, M. "Simultaneous impact of nonlinear radiative heat flux and Arrhenius activation energy in flow of chemically reacting Carreau nanofluid." *Applied Nanoscience* 10 (2020): 2977–2988. https://doi.org/10.1007/s13204-019-01012-6

[32] Patel, Manoj R., Jigisha U. Pandya, and Vijay K. Patel. "Numerical analysis of fluid flow behaviour in two sided deep lid driven cavity using the finite volume technique." *Computational Methods for Differential Equations* (2022). https://doi.org/10.22034/cmde.2022.49864.2074

[33] Muhammad, T., Alamri, S. Z., Waqas, H., Habib, D. and Ellahi, R. "Bioconvection flow of magnetized Carreau nanofluid under the influence of slip over a wedge with motile microorganisms." *Journal of Thermal Analysis and Calorimetry* 143 (2021): 945-957. https://doi.org/10.1007/s10973-020-09580-4

[34] Hamrelaine, Salim, Fateh Mebarek-Oudina, and Mohamed Rafik Sari. "Analysis of MHD Jeffery Hamel flow with suction/injection by homotopy analysis method." *Journal of Advanced Research in Fluid Mechanics and Thermal Sciences* 58, no. 2 (2019): 173-186.

[35] Patel, Manoj R., Jigisha U. Pandya, and Vijay K. Patel. "Numerical Analysis of Fluid Flow Behaviour in Four-Sided Square Lid-Driven Cavity Using the Finite Volume Technique." *International Journal of Applied and Computational Mathematics* 8, no. 4 (2022): 1-23. https://doi.org/10.1007/s40819-022-01353-x

[36] Ismail, Mohamad Alif, Mohamad Hidayad Ahmad Kamal, Lim Yeou Jiann, Anati Ali, and Sharidan Shafie. "Transient Free Convection Mass Transfer of Second-grade Fluid Flow with Wall Transpiration." *CFD Letters* 13, no. 11 (2021): 35-52. https://doi.org/10.37934/cfdl.13.11.3552

[37] Roja, P., T. Sankar Reddy, S. M. Ibrahim, G. Lorenzini, and Nor Azwadi Che Sidik. "The Effect of Thermophoresis on MHD Stream of a Micropolar Liquid Through a Porous Medium with Variable Heat and Mass Flux and Thermal Radiation." *CFD Letters* 14, no. 4 (2022): 118-136. https://doi.org/10.37934/cfdl.14.4.118136

[38] Hayat, T., Bibi, A., Yasmin, H. and Alsaadi, F.E. "Magnetic Field and Thermal Radiation Effects in Peristaltic Flow with Heat and Mass Convection." *J of Thermal Sci Eng Appl* 10 (2018): 051018. https://doi.org/10.1115/1.4040282
[39] Zeeshan, A., Hussain, F., Ellahi, R. and Vafai, K. "A study of gravitational and magnetic effects on coupled stress bi-phase liquid suspended with crystal and Hafnium particles down in steep channel." *Journal of Molecular Liquids* 286 (2019): 110898. https://doi.org/10.1016/j.molliq.2019.110898
[40] Khan, W.A., Sultan, F., Ali, M., Shahzad, M., Khan, M. and Irfan, M. "Consequences of activation energy and binary chemical reaction for 3D flow of Cross-nanofluid with radiative heat transfer." *Journal of the Brazilian Society of Mechanical Sciences and Engineering* 41 (2019): 4. https://doi.org/10.1007/s40430-018-1482-0
[41] Sandeep, N. and Sulochana, C. "Momentum and heat transfer behaviour of Jeffrey, Maxwell and Oldroyd-B nanofluids past a stretching surface with non-uniform heat source/sink." *Ain Shams Engineering Journal* 9, no. 4 (2018): 517–524. https://doi.org/10.1016/j.asej.2016.02.008
[42] Acharya, N., Bag, R. and Kundu, P.K. "Influence of Hall current on radiative nanofluid flow over a spinning disk: a hybrid approach." *Physica E* 111 (2019): 103–112. https://doi.org/10.1016/j.physe.2019.03.006
[43] Ali, M., Khan, W.A., Irfan, M., Sultan, F., Shahzed, M. and Khan, M. "Computational analysis of entropy generation for cross-nanofluid flow." *Applied Nanoscience* 10 (2020): 3045–3055. https://doi.org/10.1007/s13204-019-01038-w
[44] Nazeer, M., Ali, N., Ahmad, F., Ali, W., Saleem, A., Ali, Z., Sarfraz, A. "Effects of radiative heat flux and joule heating on electro-osmotically flow of non-Newtonian fluid Analytical approach." *International Communications in Heat and Mass Transfer* 117 (2020): 104744. https://doi.org/10.1016/j.icheatmasstransfer.2020.104744
[45] Nazeer, M., Khan, M.I., Rafiq, M.U. and Khan, N.B. "Numerical and scale analysis of Eyring-Powell nanofluid towards a magnetized stretched Riga surface with entropy generation and internal resistance." *International Communications in Heat and Mass Transfer* 119 (2020): 104968. https://doi.org/10.1016/j.icheatmasstransfer.2020.104968
[46] Firdous, H., Husnine, S.M., Hussain, F., Nazeer, M. "Velocity and thermal slip effects on two-phase flow of MHD Jeffrey fluid with the suspension of tiny metallic particles." *Physica Scripta* 96 (2021): 025803. https://doi.org/10.1088/1402-4896/abcff0
[47] Nadeem, S., and Akbar, N.S. "Peristaltic Flow of a Jeffrey Fluid with Variable Viscosity in an Asymmetric Channel." *Zeitschrift für Naturforschung A* 64, no. 11 (2009): 713-722. https://doi.org/10.1515/zna-2009-1107
[48] Rosseland, Svein. "Astrophysik: Auf atomtheoretischer grundlage." Vol. 11. Springer-Verlag, 2013.
[49] Hossain, M.A., Alim, M.A. and Rees, D.A.S. "The effect of radiation on free convection from a porous vertical plate." *Int J of Heat and Mass Tran* 42, no. 1 (1999): 181–191. https://doi.org/10.1016/S0017-9310(98)00097-0
[50] Liao, S. "On the homotopy analysis method for nonlinear problems." *Applied Mathematics and Computation* 147, no. 2 (2004): 499–513. https://doi.org/10.1016/S0096-3003(02)00790-7
[51] Hayat, T., Ijaz, M.K., Alsaedi, A. and Imran, M.K. "Joule heating and viscous dissipation in flow of nanomaterial by a rotating disk." I*nternational Communications in Heat and Mass Transfer* 89 (2017): 190–197. https://doi.org/10.1016/j.icheatmasstransfer.2017.10.017
[52] Qayyum, S., Ijaz, M.K., Hayat, T., Alsaedi, A. and Tamoor, M. "Entropy generation in dissipative flow of Williamson fluid between two rotating disks." *International Journal of Heat and Mass Transfer* 127, Part C (2018): 933–942. https://doi.org/10.1016/j.ijheatmasstransfer.2018.08.034
[53] Waqasa, M, Shehzad, S.A., Hayat, T., Ijaz, M.K. and Alsaedi, A. "Simulation of magnetohydrodynamics and radiative heat transport in convectively heated stratified flow of Jeffrey nanofluid." *Journal of Physics and Chemistry of Solids* 133, (2019): 45–51. https://doi.org/10.1016/j.jpcs.2019.03.031
[54] Liao, Shijun, ed. *Advances in the homotopy analysis method*. World Scientific, 2013. https://doi.org/10.1142/8939
[55] Vajravelu, Kuppalapalle, and R. Van Gorder. *Nonlinear flow phenomena and homotopy analysis*. Berlin: Springer, 2013. https://doi.org/10.1007/978-3-642-32102-3
[56] Chen, C-H. "Laminar mixed convection adjacent to vertical, continuously stretching sheets." *Heat and Mass transfer* 33, no. 5 (1998): 471-476. https://doi.org/10.1007/s002310050217
[57] Andersson, H. I., K. H. Bech, and B. S. Dandapat. "Magnetohydrodynamic flow of a power-law fluid over a stretching sheet." *International Journal of Non-Linear Mechanics* 27, no. 6 (1992): 929-936. https://doi.org/10.1016/0020-7462(92)90045-9
[58] Chen, Chien-Hsin. "Effects of magnetic field and suction/injection on convection heat transfer of non-Newtonian power-law fluids past a power-law stretched sheet with surface heat flux." *International Journal of Thermal Sciences* 47, no. 7 (2008): 954-961. https://doi.org/10.1016/j.ijthermalsci.2007.06.003